

Covariant Active-Hydrodynamics of Shape-Changing Epithelial Monolayers

Richard G. Morris and Madan Rao

*Simons Centre for the Study of Living Machines, National Centre for Biological Sciences,
Tata Institute for Fundamental Research, Bangalore, 560065, India.*

During the early-stages of embryo development, morphogenesis—the emergence of shape and form in living organisms—is almost exclusively associated with monolayers of tightly bound epithelial cells. To understand how such tissues change their shape, we construct a fully covariant active-hydrodynamic theory. At the cellular scale, stresses arise from apical contractility, mechanical response and the constraint of constant cell volume. Tissue-scale deformations emerge due to the balance between such cell-autonomous stresses and the displacement and shear of a low Reynolds number embedding fluid. Tissues with arbitrary curvature or shape can be described, providing a general framework for epithelial monolayer morphology. Analysis of the stability of flat monolayers reveals two generic shape instabilities: passive constrained-buckling, and actively-driven tissue deformation. The active instability can be further categorised into two types, corresponding to cell shape changes that are either “squamous to columnar” or “regular-prism to truncated-pyramid”. The deformations resulting from the latter qualitatively reproduce *in vivo* observations of the onset of both mesoderm and posterior midgut invaginations, which take place during gastrulation in the fruit fly *Drosophila melanogaster*.

Morphogenesis—the autonomous formation of shape and form—is a profound process that has fascinated scientists since long before d’Arcy Thompson’s treatise on the subject one hundred years ago [1]. In the context of early-embryo development, the archetypal tissues responsible for such deformations are aggregates of epithelial cells, typically arranged in thin sheets [2]. One of the most striking examples, and a system subject to intense experimental research, is the process of gastrulation in the fruit fly *Drosophila melanogaster* [3, 4]. Here, the epithelium—a monolayer of cells, tightly connected to each other via proteins such as E-cadherin—undergoes embryo-scale deformations which form the basis of the fly’s anatomy [5]. We focus on the mesoderm and posterior midgut invaginations (see Fig. 1) where shape changes arise as a result of constricting the apical surface of the individual epithelial cells; itself attributed to the action of myosin-II motors on an especially dense cortical layer of actin that underpins the apical surface [6–8]. On the timescale of such deformations, there is neither proliferation nor cell death, and cells retain the same neighbours. The latter prohibits both the flow of cells relative to each other and actively-mediated topological changes, such as the T1-transition.

Our approach is to use a coarse-grained active-hydrodynamic description (in the generalised sense of [9, 10]), where cells are “microscopic” quantities. Here, whether relating to gastrulation or some other aspect of developmental morphogenesis, changes in tissue geometry are a defining (and inescapable) feature which must be characterised. As a result, our treatment is necessarily covariant; cast in the language of differential geometry. A key assumption is to exploit the fact that the lateral scale of epithelial monolayers is an order of magnitude larger than the thickness¹ and invoke a “thin film” ap-

proximation, where the epithelium is represented by a single time-dependent manifold that separates two identical semi-infinite low-Reynold-number fluids. The theoretical context is therefore the body of work that spans deformations of passive fluid membranes [11, 12] and, more recently, *active* membranes [13, 14].

In the embryonic setting, forces generated by the epithelium are balanced by the displacement and shear of the highly viscous yolk, or embedding fluid, which is the dominant method of dissipation [see [15, 16] and Supporting Information (SI)]. Such forces are typically functions of local geometry (*e.g.*, stretching or bending) and have both passive and active contributions. The former is written in terms of an effective free-energy density that captures the mechanical response of cells (*e.g.*, apical, basal and lateral faces, enclosing an incompressible volume [17]). The latter is assumed to be generated by the ubiquitous machinery of the contractile acto-myosin cortex, therefore requiring an auxiliary equation for the dynamics of an excitable scalar field for the density of myosin-II motors bound to each cell cortex.

In the following, we expand on the above and present a quantitative framework to address the leading-order physics of tissue shape changes. Our closed-form theory is, in principle, very general, and able to describe arbitrary shape changes. In practice, however, the treatment of complex geometries and non-linearities typically requires a numerical implementation. We therefore validate our framework by analysing the stability of flat steady-state (contractile) monolayers. Notably, even such an ostensibly straightforward setting gives rise to a rich set of behaviours, including a novel passive *constrained*-buckling, and an active *invaginating* instability that is reminiscent of the onset of both mesoderm

¹ The semi-major and semi-minor axis of the embryo have typical

lengths $\sim 200 \mu m$ and $\sim 150 \mu m$, respectively. The typical lateral thickness of the epithelial cells are $\sim 10 \mu m$.

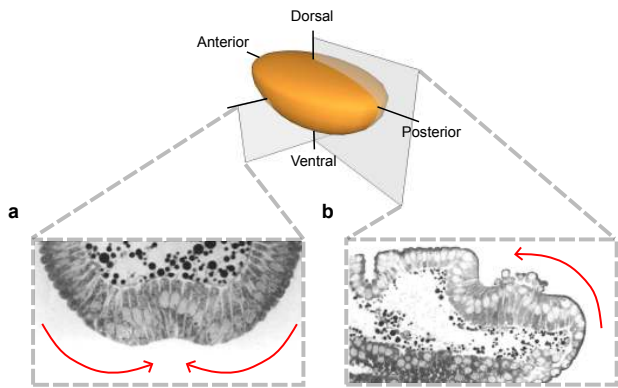


FIG. 1. **Shape-changing tissues.** Gastrulation in the fruit fly *Drosophila melanogaster* is characterised by two canonical invaginations, where epithelial monolayers autonomously change their shape with unerring accuracy and robustness. The mesoderm invagination spans the anterior-posterior axis on the ventral side (a), whilst the midgut invagination begins at the posterior pole and progresses towards the anterior along the dorsal side (b). Bright-field images are reproduced with permission from [3].

and midgut invaginations seen during gastrulation of the model organism *Drosophila Melanogaster*.

I. MORPHOLOGY

Focussing first on the surface of connected apical faces, we use an “internal”, Lagrangian, coordinate $u \in \mathbb{R}^2$ to label fixed points (*e.g.*, a given junction between three cells). The *positions* of these points $\mathbf{R}(u, t) \in \mathbb{R}^3$ then form a manifold \mathcal{S}_t , which is just the image of u under a time-dependent embedding, $\mathbf{R}_t : \mathbb{R}^2 \rightarrow \mathbb{R}^3$ (see Fig. 2). It is the structure of \mathcal{S}_t , induced on the domain \mathbb{R}^2 of u , which is of interest. In particular, the metric, $g_{\alpha\beta}(u, t) = \mathbf{R}_{,\alpha} \cdot \mathbf{R}_{,\beta}$, which encodes local strains, and the coefficients of the second-fundamental form, $b_{\alpha\beta}(u, t) = \hat{\mathbf{n}} \cdot \mathbf{R}_{,\alpha\beta}$, which describes bending, or curvature. Here, “ \cdot ” is the usual scalar product in \mathbb{R}^3 , a subscript comma followed by an index (say, α) is shorthand for the partial derivative $\partial/\partial u^\alpha$, and $\hat{\mathbf{n}}$ is the unit normal to \mathcal{S}_t (see SI).

Assuming no lateral shear (*i.e.*, between apical and basal faces) the surface of connected basal faces can be written as a normal projection: $\mathbf{R}_B(u, t) = \mathbf{R}(u, t) - \hat{\mathbf{n}}(u, t)\ell(u, t)$, where $\ell(u, t)$ is a thickness that can vary with both position and time. We further assume that the monolayer is “thin” in the sense that $|\ell_{,\alpha}| \ll |\ell H| \ll 1$, where $H = g^{\alpha\beta} b_{\alpha\beta}/2$ is the mean curvature of the apical surface. As a result, local geometrical characteristics of the basal surface can be expressed as power-series expansions in ℓ , with coefficients that are determined by apical geometry, *e.g.*,

$$g_{\alpha\beta}^B = g_{\alpha\beta} + 2\ell b_{\alpha\beta} + \ell^2 (2H b_{\alpha\beta} - K g_{\alpha\beta}) + O(\ell^3), \quad (1)$$

where $K = b/g$ is the Gaussian curvature [the notation

$g = \det(g_{\alpha\beta})$ and $b = \det(b_{\alpha\beta})$ is used throughout]. In this approximation, therefore, we need only consider the dynamics of a single manifold—the apical surface \mathcal{S}_t —and the field ℓ .

As the tissue undergoes a deformation, the velocity $\mathbf{v}(u, t) = \partial\mathbf{R}(u, t)/\partial t$ at each point on the apical surface causes the coefficients $g_{\alpha\beta}$ and $b_{\alpha\beta}$ to change in time (which are, in turn, coupled to ℓ , as will be shown). The rate of such changes are most naturally expressed in terms of the components of \mathbf{v} under the decomposition $\mathbf{v} = v^\alpha \mathbf{R}_{,\alpha} + v^{(n)} \hat{\mathbf{n}}$ —*i.e.*, tangent- and normal-to \mathcal{S}_t (see Fig. 2). Leaving the details to the SI, we have

$$\partial_t g_{\alpha\beta} = v_{\alpha;\beta} + v_{\beta;\alpha} - 2v^{(n)} b_{\alpha\beta}, \quad (2)$$

and

$$\begin{aligned} \partial_t b_{\alpha\beta} = & v^\gamma b_{\alpha\beta,\gamma} + b_{\alpha\gamma} v^\gamma_{,\beta} + b_{\gamma\beta} v^\gamma_{,\alpha} + v^{(n)}_{,\alpha;\beta} \\ & - v^{(n)} (2H b_{\alpha\beta} - K g_{\alpha\beta}), \end{aligned} \quad (3)$$

respectively, where a semi-colon followed by an index is used as shorthand for the components of the covariant derivative (see SI).

We make two remarks concerning the above. First, since not every pair of first and second fundamental forms describe a surface, the symmetric, real, 2×2 matrices of coefficients $g_{\alpha\beta}$ and $b_{\alpha\beta}$ only represent four degrees of freedom, rather than six, due to the Gauss-Codazzi relations [18]. Here, such conditions need not be explicitly enforced so long as $\mathcal{S}_{t=0}$ is well defined, since compatibility with Gauss-Codazzi is preserved under the action of Eqs. (2) and (3). Second, there is no need for an additional equation for the time dependence of the number density of cells, $\rho(u, t) = \rho(u, 0)/\sqrt{g}$. By taking the determinant of Eq. (2), followed by the square root, we can deduce that

$$\partial_t \rho + \rho v^\alpha_{;\alpha} - 2\rho v^{(n)} H = 0. \quad (4)$$

This is precisely the equation for a conserved scalar field associated with a moving manifold [18, 19], but without the standard convective term $v^\alpha \rho_{,\alpha}$, which does not appear because, by construction, there is neither proliferation nor death and cells cannot flow relative to the internal coordinate u (*cf.* Ref. [20]).

II. BALANCE OF FORCES

The velocity field \mathbf{v} —required to close Eqs. (2) and (3)—is prescribed by a balance of forces: equating the dissipative forces of the Stokesian embedding fluid to those generated in the epithelium. Ignoring any hydrodynamic affects that arise due to finite thickness, the impermeable nature of the tissue relates \mathbf{v} to the per-unit-area epithelial forces \mathbf{f} (applied *on* the fluid *by* the tissue) via convolution with the (three dimensional) Os-

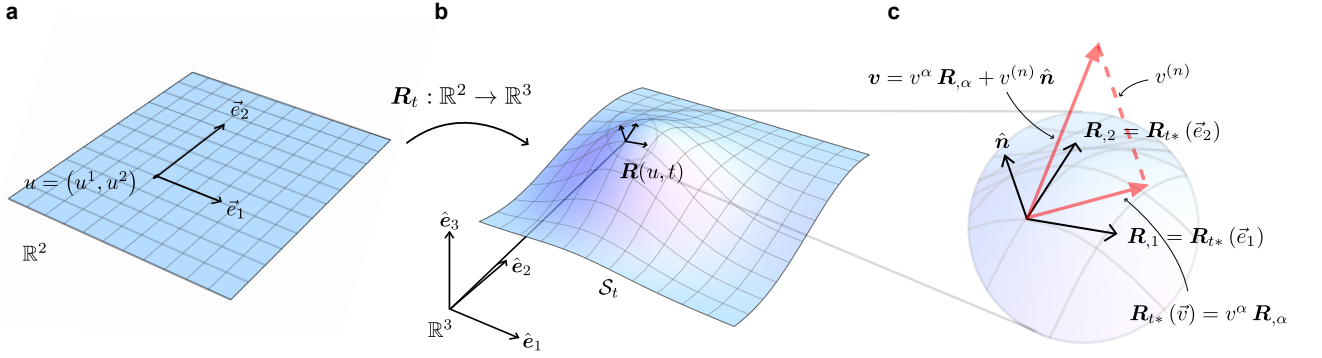


FIG. 2. **Deforming manifolds.** The surface of connected apical faces is parameterised by an Lagrangian coordinate $u \in \mathbb{R}^2$, whose domain is spanned by \vec{e}_α (a). Under the time-dependent embedding $\mathbf{R}_t : \mathbb{R}^2 \rightarrow \mathbb{R}^3$, the positions of points $\mathbf{R}(u, t) \in \mathbb{R}^3$ form the manifold S_t (b). At a given point, the tangent space $T_{\mathbf{R}(u, t)} S_t$ is spanned by $\mathbf{R}_{t*}(\vec{e}_\alpha) = \mathbf{R}_{, \alpha}$. Under deformation, the local velocity $\mathbf{v} = \partial \mathbf{R}(u, t) / \partial t$ can be decomposed into tangential and normal components: $\mathbf{v} = v^\alpha \mathbf{R}_{, \alpha} + v^{(n)} \hat{\mathbf{n}}$ (c).

een tensor [21, 22]

$$\mathbf{v}(\mathbf{R}(u, t)) = \int_{\mathbb{R}^2} du' \mathbf{O}(\mathbf{R}(u', t) - \mathbf{R}(u, t)) \cdot \mathbf{f}(\mathbf{R}(u', t)). \quad (5)$$

The forces \mathbf{f} can be decomposed into both active and passive-like contributions. Here, passive-like is used as shorthand for dynamical behaviour that is characterised by a Lyapounov functional, in analogy with the free-energy of a passive system. We write

$$\mathcal{F} = \int_{\mathbb{R}^2} F(g_{\alpha\beta}, b_{\alpha\beta}, \ell) \text{vol}^2, \quad (6)$$

where $\text{vol}^2 = \sqrt{g} du^1 \wedge du^2$ is the induced volume form on \mathbb{R}^2 (see SI) and F is an *effective* free-energy density (per unit area). The primary mechanical response of a tissue is elastic-like, with restoring forces that are linear in strain (see Fig. 3). Contributions from apical, basal and lateral faces are encoded by five moduli: isotropic and symmetric non-isotropic coefficients for each of the apical (λ_A and μ_A) and basal (λ_B and μ_B) sides, and a single coefficient κ associated with the tissue thickness. In principle, such quantities may rely on the concentrations of passive cross-linkers, cell-cell adhesions or other actively-regulated molecules and could even be space-time dependent. However, for the purposes of this article they are treated as constant (therefore resembling Lamé coefficients of the first- and second-kind).

Introducing the time-independent matrices $g_{\alpha\beta}^\dagger$ and $g_{\alpha\beta}^{\text{B}\dagger}$ to represent the reference configurations of apical

and basal surfaces respectively, the coefficients of the corresponding Green-Lagrange strain 2-forms [18, 19] are then $\epsilon_{\alpha\beta} = g_{\alpha\beta} - g_{\alpha\beta}^\dagger$ and $\epsilon_{\alpha\beta}^{\text{B}} = g_{\alpha\beta} - g_{\alpha\beta}^{\text{B}\dagger} - 2\ell b_{\alpha\beta} + \ell^2(2H b_{\alpha\beta} - K g_{\alpha\beta}) + O(\ell^2)$ (see SI). By analogy with both active elastomers [23, 24] and discrete (3D) vertex models [17, 25, 26] the effective free-energy is taken to be of the form

$$F = \mu_A \bar{\epsilon}_{\alpha\beta} \bar{\epsilon}^{\alpha\beta} + \lambda_A [\text{Tr}_g(\epsilon_{\alpha\beta})]^2 + \mu_B \bar{\epsilon}_{\alpha\beta}^{\text{B}} \bar{\epsilon}^{\alpha\beta} + \lambda_B [\text{Tr}_{g_{\text{B}}}(\epsilon_{\alpha\beta}^{\text{B}})]^2 + \kappa(\ell - \ell^\dagger)^2, \quad (7)$$

where ℓ^\dagger is the reference thickness, and an overbar is used to denote the symmetric traceless part, *i.e.*, $\bar{\epsilon}_{\alpha\beta} = \epsilon_{\alpha\beta} - g^{\alpha\beta} \text{Tr}_g(\epsilon_{\alpha\beta}) / 2^2$.

We assume that the relaxation of the lateral cell faces is orders of magnitude faster than either the apical or basal faces, due to a lower density of cortical cytoskeleton, implying $\delta\mathcal{F}/\delta\ell = 0^3$. The minimisation is performed under the constraint that, on the timescales of the midgut invagination, the volume enclosed by epithelial cells is incompressible. That is, the local constraint $V \simeq \ell \sqrt{g}(1 - \ell H) + O(\ell^3)$, must be satisfied everywhere (see SI) where the $V(u)$ is the time-independent volume of a patch containing $\rho(u, 0) \sqrt{g}(u, 0)$ cells.

Using the above to eliminate ℓ (in terms of $g_{\alpha\beta}$, $b_{\alpha\beta}$, and material parameters), it is the remaining functional behaviour of \mathcal{F} that contributes to (5) via

$$\mathbf{f} = -\frac{\delta\mathcal{F}}{\delta\mathbf{R}} + \nabla \cdot \sigma, \quad (8)$$

where σ is an active stress and $\nabla = \mathbf{R}_{, \alpha} g^{\alpha\beta} \partial_\beta$ is the gradient operator associated with S_t . The term $\delta\mathcal{F}/\delta\mathbf{R}$ may be unpacked (see SI and [27]) to give

$$\frac{\delta\mathcal{F}}{\delta\mathbf{R}} = \left[-\pi^{\alpha\beta}{}_{;\beta} - (b^\alpha{}_\gamma \psi^{\gamma\beta})_{;\beta} - b^\alpha{}_\gamma \psi^{\gamma\beta}{}_{;\beta} \right] \mathbf{R}_{, \alpha} + \left[-\pi^{\alpha\beta} b_{\alpha\beta} - \psi^{\alpha\beta} (2H b_{\alpha\beta} - K g_{\alpha\beta}) + \psi^{\alpha\beta}{}_{;\alpha\beta} \right] \hat{\mathbf{n}}, \quad (9)$$

where

$$\pi^{\alpha\beta} = \frac{1}{\sqrt{g}} \frac{\partial(\sqrt{g}F)}{\partial g_{\alpha\beta}}, \text{ and } \psi^{\alpha\beta} = \frac{\partial F}{\partial b_{\alpha\beta}}. \quad (10)$$

In a similar way, the active term may also be expanded

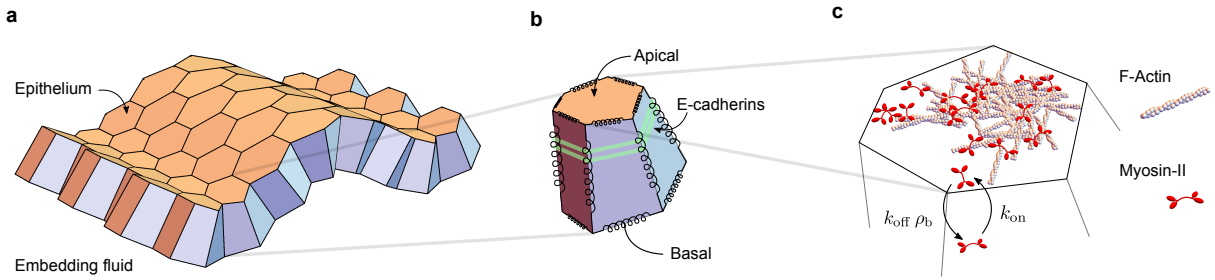


FIG. 3. **Cell-autonomous force generation.** The epithelium is a monolayer of epithelial cells (a). Each cell is in the shape of a hexagonal prism, with the apical side facing out of the embryo and the basal side facing inwards (b). Cells enclose a fixed (time-independent) volume, and are tightly bound to each other by a localised belt of E-cadherin proteins (cell-cell adhesions) on the lateral faces. The (active) mechanical response of cells to an applied stress is assumed to be linear [and hence indicated by a spring (b)], in-line with measurements of recoil following laser ablation. The action of myosin-II motors on the dense layer of cortical actin that underpins the apical cell faces leads to contractile stresses (c).

to give

$$\nabla \cdot \sigma = (\sigma^{\alpha\beta}{}_{;\beta}) \mathbf{R}_{,\alpha} + (\sigma^{\alpha\beta} b_{\alpha\beta}) \hat{\mathbf{n}}. \quad (11)$$

Such forces act at the apical surface only, consistent with experimental observations. If necessary, the effects of active basal stresses can be incorporated via “normal projection”, in the same way as for the effective free energy.

For the components of σ , we make the standard assumption of an unlimited background reservoir of ATP, the hydrolysis of which is maintained at a constant chemical potential gradient $\Delta\mu_{\text{ATP}} > 0$, driving contractility. The stresses that deform the local actin meshwork assume the generic form

$$\sigma^{\alpha\beta} = \chi(\rho, \rho_b) \Delta\mu_{\text{ATP}} g^{\alpha\beta}, \quad (12)$$

where χ is a compressibility that not only relies on the density of cells, ρ , but also the density of apically bound myosin-II, ρ_b (see Fig. 3). The scalar field ρ_b is non-conserved and drives tangent-plane contractility at the apical surface. As a first approximation, we assume simple Langmuir-like kinetics, where myosin-II filaments bind to apical actin from the bulk of a cell with a rate k_{on} , and unbind at a rate which is proportional to the current density $k_{\text{off}}\rho_b$. The resulting continuity equation is therefore modified to

$$\partial_t \rho_b + (\rho_b v^\alpha)_{;\alpha} - \rho_b v^{(n)} 2H = k_{\text{on}} - k_{\text{off}}\rho_b. \quad (13)$$

III. HYDRODYNAMIC INSTABILITIES

The system of equations (2), (3) and (13) describe the dynamical behaviour of five degrees-of-freedom (the remaining equations are constitutive, describing \mathbf{v} as a function of ρ_b , $g_{\alpha\beta}$ and $b_{\alpha\beta}$). The treatment is fully-covariant and capable of describing arbitrary tissue deformations so long as they do not change the topology of the apical manifold (*e.g.* by introducing holes or handles). Due to their inherent non-linear nature, however, the closed system of PDEs we present cannot be solved analytically. Nevertheless, the system is, in principle, amenable to numerical implementation via the use of coordinate-free finite-element methods [28, 29]. Such an approach also allows the study (and visualisation) of complex geometries, permitting much greater comparison with experiment. Leaving this task for further work, the remainder of this article is dedicated to the study of characteristic behaviours by employing linear stability analysis.

For simplicity, the analysis is restricted to deformations that are confined to a single plane (so-called “quasi-1D”), reducing the number of dynamical degrees-of-freedom to three—*e.g.*, \sqrt{g} , H and ρ_b . In this simplified setup, we consider the stability (in Fourier space [30]) of perturbations from a flat, up/down symmetric, steady state at time $t = 0$ [*i.e.*, $b_{\alpha\beta}(u, 0) = 0$ for all u]. For convenience, we assume that the rest configurations of apical and basal surfaces are equal ($g_{\alpha\beta}^{\text{B}\dagger} = g_{\alpha\beta}^{\dagger}$) and that the Lamé-like coefficients are also equal ($\lambda_A = \lambda_B =: \lambda$ and $\mu_A = \mu_B =: \mu$). This ensures that no torque need be applied at the tissue boundary in order to keep it flat. We do, however, apply an in-plane force at the boundary. The reason is that, although flat, the tissue is active: there is a homogeneous steady-state concentration of bound myosin-II $\rho_b(u, 0)$, which leads to homogeneous contractile stresses. We choose the boundary force to be such that the (homogeneous) metric at steady state, $g_{\alpha\beta}(u, 0)$, is the same as the rest metric

² Certain vertex models include an interfacial contribution, proportional to the total area of the lateral faces [17, 25]. However, there is little experimental evidence to suggest such terms contribute to the energetics at lowest order, therefore they are omitted here for simplicity.

³ To incorporate a finite timescale of thickness relaxation, we must use $\partial_t \ell = -\Gamma \delta\mathcal{F}/\delta\ell + \text{active terms}$.

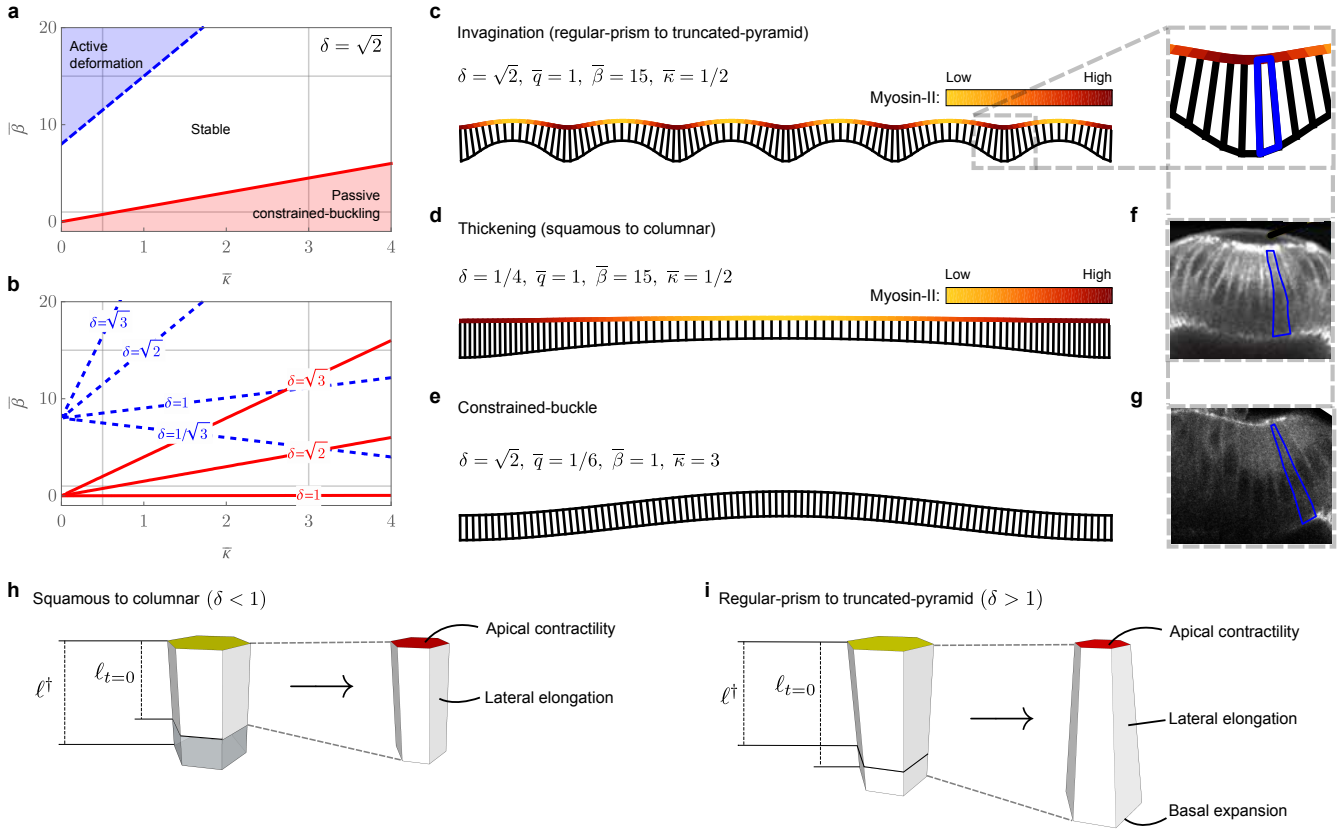


FIG. 4. Hydrodynamic instabilities reproduce the key features observed during the onset of invaginations. Two classes of instability can be identified (a): passive constrained-buckling and active deformation. The latter can be further categorised into two sub-types: invaginating and thickening [(c) and (d), respectively]. Boundaries between stable and unstable configurations are controlled by $\delta = \ell_{t=0}/\ell^\dagger$, with the constrained-buckling instability disappearing for all $\delta \leq 1$ (b). Geometrically faithful schematics of active [(a) and (b)] and passive (c) instabilities can be constructed (see SI). For the former, the concentration of apical myosin-II is shown via a colormap, ranging from yellow (low concentration) to red (high concentration). In terms of cellular shape changes, the invaginating and thickening instabilities are characterised by “regular-prism to truncated-pyramid” (i) and “squamous to columnar” (h) transitions, respectively. The invaginating instability (c) qualitatively reproduces the key features of both mesoderm (f) and midgut (g) invaginations, observed using multi-photon microscopy of regulatory light-chain-GFP labelled myosin. Increased myosin density [shown in white in (f) and (g)] at the apical surface correlates with constriction of the cell faces resulting in both lateral and basal extension. The former thickens the Epithelium whilst the latter causes splay and hence induces curvature. Image (f) was reproduced from [31] with permission, whilst image (g) was kindly contributed by T. Lecuit, C. Collinet and A. Bailles (see Acknowledgements).

$g_{\alpha\beta}^\dagger$. The coordinates u may then be chosen such that $g_{\alpha\beta}(u, 0) = g_{\alpha\beta}^\dagger = \delta_{\alpha\beta}$.

Consigning the details to the SI, the results are shown in Fig. 4. Here, instabilities are given in terms of a dimensionless measure of active contractility, $\bar{\beta} := \chi^{(0)} \Delta\mu_{\text{ATP}} / (\lambda + \mu/2)$, and a dimensionless (elastic-like) response due to changes in thickness, $\bar{\kappa} := \kappa (\ell^\dagger)^2 / (\lambda + \mu/2)$. The boundary between stable and unstable regions is characterised by a dimensionless “pre-strain” $\delta = \ell(u, 0)/\ell^\dagger$ —*i.e.*, the steady state ($t = 0$) strain of the lateral faces. Given the implied boundary force described above, this is tantamount to choosing the volume enclosed by each cell.

For comparatively low $\bar{\beta}/\bar{\kappa}$, the tissue is unstable to passive *constrained-buckling* (below the solid red line of Fig. 4a). The instability only exists for $\delta > 1$ —*i.e.*,

when the lateral faces are extended at steady state—and is contrary to predictions of traditional un-constrained buckling [17], based on energy minimisation arguments. Constrained-buckling (Fig. 4e and SI) is a *finite* wave-number effect seen, for example, in poroelastic rods [32] and microtubules in living cells [33]. Here, the characteristic wave-number of the buckle is non-zero due to the combined effects of basal and lateral elasticity. The former imposes an effective bending energy $\sim \delta (\lambda + \mu/2)$, suppressing basal expansion and therefore buckling at large wave-number. For the latter, the low curvature deformations at small wave-number require lateral extension, with an energy cost $\sim \kappa$.

For comparatively high $\bar{\beta}/\bar{\kappa}$, *active* deformations are unstable (above the dashed blue line of Fig. 4a) and correspond to a contractile instability at the apical surface,

driven by variations in ρ_b . However, the effect that this has on cell shapes, and hence the overall tissue deformation, depends on δ .

For $\delta \leq 1$, the lateral faces are under compression, and cells respond to apical contraction by elongation—*i.e.*, a squamous to columnar transition. Here, the shape of the apical surface remains unchanged, whilst the thickness is inversely proportional to apical contractility, vanishing as wave-number approaches zero (Fig. 4d and SI).

By contrast, if $\delta > 1$, the lateral faces are already under strain. As a result, myosin-driven apical constriction leads not only to lateral extension, but also to an expansion of the basal face—*i.e.*, a regular-prism to truncated-pyramid transition. The corresponding tissue-scale deformations (Fig. 4c and SI) qualitatively resemble early-onset invaginations seen during *Drosophila* gastrulation (Figs. 4f and 4g). This result is also clearly in-line with *in vivo* cellular tomography, where two-photon scanning microscopy images of E-cadherin-GFP mutants permits the high-fidelity three-dimensional reconstruction of cell shapes [34]. Here, apical constriction of cells at the mesoderm invagination results in cell shapes that are extended both laterally and basally, whilst keeping cell volume constant.

IV. DISCUSSION

In summary, we use a thin-film approximation and differential geometry to capture the salient physical features of epithelial monolayer morphology: apical contractility; mechanical response; and a momentum-conserving embedding fluid (Fig. 3). While our general treatment allows us to deal with tissues of arbitrary curvature, analysis in a restricted scenario identifies three distinct hydrodynamic instabilities that are qualitatively in-line with experimental evidence. We envisage such regimes to be common across a broad range of deforming tissues.

Importantly, our approach sets the foundations for further refinements in the understanding of tissue physics. Many outstanding questions can be addressed within the context of the framework set out here, for example: what happens in more complex geometries (*e.g.*, in systems where the steady-state symmetry is broken); how is the mechanical response of a tissue actively regulated (*e.g.*, how do κ and the four Lamé-like coefficients rely on ρ_b); what is the role, if any, of active interfacial dynamics

between lateral faces (*e.g.*, [35]); how do cells modulate their behaviour in response to mechanical cues, such as stress, strain, or strain-rate (*e.g.*, how do the rates k_{on} and k_{off} rely on $\epsilon_{\alpha\beta}$, $\pi^{\alpha\beta}$ *etc.*), and; what is the role of the embedding fluid, and other global constraints such as the surrounding inextensible vitelline membrane.

Experimentally, advances in *in vivo* imaging [36, 37] combined with classical genetics and state-of-the-art mechano-biology manipulations (*e.g.*, laser-ablation and laser-induced cauterisation) are leading renewed interest in the behaviour of tissues during development [38, 39], suggesting that a data-led approach to such questions will soon be within reach. In this context, our closed-form dynamical theory provides a quantitative framework which, due to its covariant nature, can be used in conjunction with data concerning shape changes such as movement, compression, folding, and invagination. That is, over and above the presented linear stability analysis, we expect a numerical implementation of the full non-linear theory to prove a useful tool for understanding the increasingly sophisticated experiments of developmental biology.

V. ACKNOWLEDGEMENTS

We thank Simons Foundation (USA) for financial support. For detailed discussion, and the contribution of the image used in Fig. 4g, we thank T. Lecuit, C. Collinet and A. Bailles from IBDM, Université Aix-Marseille. We acknowledge the CNRS (Laboratoire International Associé between IBDM and NCBS) for associated travel support. We also thank S. Gadgil (IISc), K. Husain, A. Rautu and A. Singh (all NCBS) for helpful discussions.

VI. AUTHOR CONTRIBUTIONS

RGM and MR conceived of the project and wrote the manuscript together. RGM performed research and analysis, with guidance from MR.

VII. COMPETING FINANCIAL INTERESTS

The authors declare no conflict of interest.

-
- [1] Thompson DW (1917) *On Growth and Form*. (Cambridge University Press, Cambridge, England).
 [2] Guillot C, Lecuit T (2013) Mechanics of Epithelial Tissue Homeostasis and Morphogenesis. *Science* (80-.). 340(6137):1185–1189.
 [3] Sweeton D, Parks S, Costa M, Wieschaus E (1991) Gastrulation in *Drosophila*: the formation of the ventral furrow and posterior midgut invaginations. *Development*

- 112(3):775–89.
 [4] Gilmour D, Rembold M, Leptin M (2017) From morphogen to morphogenesis and back. *Nature* 541(7637):311–320.
 [5] Alberts B, et al. (1989) *Molecular biology of the cell*. (Garland Science, New York).
 [6] Sherrard K, Robin F, Lemaire P, Munro E (2010) Sequential Activation of Apical and Basolateral Contractil-

- ity Drives Ascidian Endoderm Invagination. *Curr. Biol.* 20(17):1499–1510.
- [7] Lecuit T, Lenne PF, Munro E (2011) Force Generation, Transmission, and Integration during Cell and Tissue Morphogenesis. *Annu. Rev. Cell Dev. Biol.* 27(1):157–184.
- [8] He B, Doubrovinski K, Polyakov O, Wieschaus E (2014) Apical constriction drives tissue-scale hydrodynamic flow to mediate cell elongation. *Nature* 508(7496):392–396.
- [9] Marchetti MC, et al. (2013) Hydrodynamics of soft active matter. *Rev. Mod. Phys.* 85(3):1143–1189.
- [10] Ramaswamy S (2010) The Mechanics and Statistics of Active Matter. *Annu. Rev. Condens. Matter Phys.* 1(1):323–345.
- [11] Cai W, Lubensky T (1995) Hydrodynamics and dynamic fluctuations of fluid membranes. *Phys. Rev. E* 52(4):4251–4266.
- [12] Arroyo M, DeSimone A (2009) Relaxation dynamics of fluid membranes. *Phys. Rev. E* 79(3):31915.
- [13] Maitra A, Srivastava P, Rao M, Ramaswamy S (2014) Activating Membranes. *Phys. Rev. Lett.* 112(25):258101.
- [14] Salbreux G, Jülicher F (2017) Mechanics of active surfaces. *Phys. Rev. E* 96(3):032404.
- [15] Wirtz D (2009) Particle-Tracking Microrheology of Living Cells: Principles and Applications. *Annu. Rev. Biophys.* 38(1):301–326.
- [16] Wessel AD, Gumalla M, Grosshans J, Schmidt CF (2015) The Mechanical Properties of Early *Drosophila* Embryos Measured by High-Speed Video Microrheology. *Biophys. J.* 108(8):1899–1907.
- [17] Hannezo E, Prost J, Joanny JF (2014) Theory of epithelial sheet morphology in three dimensions. *Proc. Natl. Acad. Sci.* 111(1):27–32.
- [18] Frankel T (2011) *The Geometry of Physics: An Introduction*. (Cambridge University Press, Cambridge, England), 3rd edition.
- [19] Marsden JE, Hughes TJR (1983) *Mathematical Foundations of Elasticity*. (Prentice-Hall, New Jersey).
- [20] Ranft J, et al. (2010) Fluidization of tissues by cell division and apoptosis. *Proc. Natl. Acad. Sci.* 107(49):20863–20868.
- [21] Happel J, Brenner H (1965) *Low Reynolds Number Hydrodynamics*. (Prentice-Hall, New Jersey).
- [22] Peterson MA (1996) Membrane hydrodynamics at low Reynolds number. *Phys. Rev. E* 53(1):731–738.
- [23] Banerjee S, Liverpool TB, Marchetti MC (2011) Generic phases of cross-linked active gels: Relaxation, oscillation and contractility. *EPL (Europhysics Lett.)* 96(5):58004.
- [24] Banerjee DS, Munjal A, Lecuit T, Rao M (2017) Actomyosin pulsation and flows in an active elastomer with turnover and network remodeling. *Nat. Commun.* 8(1):1121.
- [25] Alt S, Ganguly P, Salbreux G (2017) Vertex models: from cell mechanics to tissue morphogenesis. *Philos. Trans. R. Soc. B Biol. Sci.* 372(1720):20150520.
- [26] Noll N, Mani M, Heemskerk I, Streichan SJ, Shraiman BI (2017) Active tension network model suggests an exotic mechanical state realized in epithelial tissues. *Nat. Phys.*
- [27] Guven J (2004) Membrane geometry with auxiliary variables and quadratic constraints. *J. Phys. A: Math. Gen.* 37(28):L313–L319.
- [28] Tannehill JC, Anderson DA, Pletcher RH (1997) *Computational Fluid Mechanics and Heat Transfer*. (Taylor and Francis, Philadelphia), 2 edition.
- [29] Solin P, Segeth K, Dolezel I (2004) *Higher-Order Finite Element Methods*. (CRC Press, Boca Raton, Florida).
- [30] Debnath L, Bhatta D (2015) *Integral Transforms and Their Applications*. (CRC Press, Boca Raton, Florida), 3 edition.
- [31] Conte V, Ulrich F, Baum B, Muñoz, Velduis J, Brodland W, Miodownik M (2012) A Biomechanical Analysis of Ventral Furrow Formation in the *Drosophila* Melanogaster Embryo *PLoS ONE* 7(4):e34473.
- [32] Skotheim JM, Mahadevan L (2004) Dynamics of poroelastic filaments. *Proc. R. Soc. A Math. Phys. Eng. Sci.* 460(2047):1995–2020.
- [33] Brangwynne CP, et al. (2006) Microtubules can bear enhanced compressive loads in living cells because of lateral reinforcement. *J. Cell Biol.* 173(5):733–741.
- [34] Gelbart M, Bing H, Martin A, Thiberge S, Wieschaus E, Kaschube M (2012) Volume conservation principle involved in cell lengthening and nucleus movement during tissue morphogenesis *Proc. Natl. Acad. Sci. U.S.A* 109(47): 19298–19303
- [35] Bielmeier C, Alt S, Weichselberger V, La Fortezza M, Harz H, Jülicher F, Salbreux G, and Classen A-K (2016) Interface contractility between differently fated cells drives cell elimination and cyst formation *Current Biology* 26, 563–574.
- [36] Pantazis P, Supatto W (2014) Advances in whole-embryo imaging: a quantitative transition is underway. *Nat. Rev. Mol. Cell Biol.* 15(5):327–339.
- [37] Mavrikakis M, Pourquie O, Lecuit T (2010) Lighting up developmental mechanisms: how fluorescence imaging heralded a new era. *Development* 137(3):373–387.
- [38] Keller R (2012) Physical Biology Returns to Morphogenesis. *Science (80-.)*. 338(6104):201–203.
- [39] Heisenberg CP, Bellaïche Y (2013) Forces in Tissue Morphogenesis and Patterning. *Cell* 153(5):948–962.

VIII. SUPPLEMENTARY MATERIAL

IX. INTRODUCTION

This supplementary material comprises a set of calculations (including a terse summary of the necessary background and notation), the details of which would be needed in order to recapitulate the results presented in the main manuscript. Useful references regarding technical aspects are [18, 19].

X. SETUP

Consider a time-dependent manifold \mathcal{S}_t , comprising points $\mathbf{R}(u, t) =: \mathbf{R}_t(u)$ that are the image of a Lagrangian coordinate $u \in \mathbb{R}^2$ (with components u^α , for $\alpha = 1, 2$) under the embedding, $\mathbf{R}_t : \mathbb{R}^2 \rightarrow \mathbb{R}^3$. Let \vec{e}_α be basis vectors spanning $T_u\mathbb{R}^2$ (*i.e.*, the tangent space to \mathbb{R}^2 at point u), and \hat{e}_i be the usual Euclidean basis spanning $T_{\mathbf{R}(u,t)}\mathbb{R}^3$ [*i.e.*, the tangent space to \mathbb{R}^3 at point $\mathbf{R}(u, t)$, which is just \mathbb{R}^3 with the origin translated by $\mathbf{R}(u, t)$]. Throughout, we adopt the convention that Greek indices take values 1 or 2, whilst Latin indices take 1, 2, or 3. If $\mathbf{R}_{t*} : T_u\mathbb{R}^2 \rightarrow T_{\mathbf{R}(u,t)}\mathbb{R}^3$ is the pushforward of \mathbf{R}_t , then $\mathbf{R}_{t*}(\vec{e}_\alpha) = \partial\mathbf{R}(u, t)/\partial u^\alpha =: \mathbf{R}_{,\alpha}$, where a subscript comma followed by an index (say, α) is shorthand for the partial derivative $\partial/\partial u^\alpha$. Using this notation $\hat{\mathbf{n}} = (\mathbf{R}_{,1} \times \mathbf{R}_{,2}) / |\mathbf{R}_{,1} \times \mathbf{R}_{,2}|$ is the unit normal to \mathcal{S}_t . The basis of 1-forms du^α ($\alpha = 1, 2$) span $T_u^*\mathbb{R}^2$ and are dual to the \vec{e}_α , such that $du^\alpha(\vec{e}_\beta) = \delta_\beta^\alpha$, where δ_β^α is the Kronecker delta symbol.

A. Metric, raising and lowering

The embedding function \mathbf{R}_t induces a metric on \mathbb{R}^2 via the pullback \mathbf{R}_t^* . That is $g_{\alpha\beta}(u) = (\mathbf{R}_t^* \mathbf{I})(\vec{e}_\alpha, \vec{e}_\beta) = \mathbf{R}_{t*}(\vec{e}_\alpha) \cdot \mathbf{R}_{t*}(\vec{e}_\beta) = \mathbf{R}_{,\alpha} \cdot \mathbf{R}_{,\beta}$, where \mathbf{I} is the first fundamental form of \mathbb{R}^3 (*i.e.*, with coefficients δ_{ij}) and “ \cdot ” is the usual dot product of \mathbb{R}^3 . At each point $u \in \mathbb{R}^2$, the induced metric can be used to define an inner product $\langle \cdot, \cdot \rangle : T_u\mathbb{R}^2 \times T_u\mathbb{R}^2 \rightarrow \mathbb{R}$. That is, for arbitrary vectors \vec{v} and \vec{w} , we define $\langle \vec{v}, \vec{w} \rangle := v^\alpha g_{\alpha\beta} w^\beta$. Such an inner product permits the explicit identification of a vector, *e.g.*, \vec{v} , with its dual 1-form, v , by the condition $v(\vec{w}) = \langle \vec{v}, \vec{w} \rangle$, which holds for all \vec{w} . Noticing that $v(\vec{w}) = v_\alpha du^\alpha(\vec{w}) = v_\alpha w^\alpha$ and using the above definition of the inner product of two vectors implies the raising and lowering properties of the metric and its inverse [$g^{\alpha\beta} = (g_{\alpha\beta})^{-1}$], respectively. That is, $v_\alpha = g_{\alpha\beta} v^\beta$ and $v^\alpha = g^{\alpha\beta} v_\beta$. Using this property, the inner product acting on two 1-forms can be defined in a complementary way to that of the inner product on vectors:

$$\langle v, w \rangle := v_\alpha g^{\alpha\beta} w_\beta = v_\alpha w^\alpha = \langle \vec{v}, \vec{w} \rangle. \quad (14)$$

B. Volume form and wedge product

The induced (pseudo)-volume-2-form on \mathbb{R}^2 is given by

$$\text{vol}^2 = \sqrt{g} du^1 \wedge du^2, \quad (15)$$

where the shorthand $g = \det[g_{\alpha\beta}]$ has been used. Here, the symbol “ \wedge ” indicates a *wedge* product. If p and q are 1-forms, their wedge product is given by $p \wedge q = p \otimes q - q \otimes p$, from which it is clear that $p \wedge q = -q \wedge p$. More generally, the wedge product is bilinear and associative, and has the following commutation relation: if $p^{(r)}$ and $q^{(s)}$ are forms of degree r and s , respectively, then $p^{(r)} \wedge q^{(s)} = (-1)^{rs} q^{(s)} \wedge p^{(r)}$. The space of all k -forms created by taking wedge products of 1-forms is written as $\bigwedge^k T^*\mathcal{S}_t$. Such forms are *alternating* linear functionals. (Note: 0-forms and 1-forms are considered to be alternating forms, even though it is ill-defined to ask if they are skew-symmetric).

C. Covariant derivative

The covariant derivative represents the rate of change of a tensor field (at u) whilst moving along the unique geodesic that has tangent vector with pre-image \vec{y} (at u) under \mathbf{R}_{t*} . In our setup:

- When acting on a scalar field ϕ , we write

$$\nabla_{\vec{y}} \phi := \phi_{,\alpha} du^\alpha(\vec{y}), \quad (16)$$

where a subscript comma “,” is shorthand for a partial derivative, *i.e.*, $\phi_{,\alpha} := \partial\phi/\partial u^\alpha$.

- When acting on a vector $\vec{v} = v^\alpha \vec{e}_\alpha$, we write

$$\nabla_{\vec{y}} \vec{v} := \vec{e}_\alpha (v^\alpha_{;\beta}) du^\beta(\vec{y}), \quad (17)$$

where the components $v^\alpha_{;\beta}$ are given by

$$v^\alpha_{;\beta} := v^\alpha_{,\beta} + v^\gamma \Gamma_{\beta\gamma}^\alpha. \quad (18)$$

Once again, a subscript comma “,” is shorthand for a partial derivative, $v^i_{;j} := \partial v^i/\partial u^j$, whilst the $\Gamma_{\beta\gamma}^\alpha = g^{\alpha\delta} (g_{\delta\beta,\gamma} + g_{\delta\gamma,\beta} - g_{\beta\gamma,\delta})/2$ are Christoffel symbols, which define the action of the covariant derivative, via $\nabla_{\vec{e}_\alpha} \vec{e}_\beta = \vec{e}_\gamma \Gamma_{\alpha\beta}^\gamma$. Note that the shorthand $\nabla_\alpha := \nabla_{\vec{e}_\alpha}$ is frequently used in physics.

- For a 1-form, the action of the covariant derivative can be defined by demanding that the “Leibniz rule” holds. That is, if a scalar field is defined by the action of a 1-form on a vector, *i.e.*, $\phi := v(\vec{w}) = v^\alpha w_\alpha$, then

$$\nabla_\alpha (v^\beta w_\beta) = (v^\beta w_\beta)_\alpha := v^\beta_{;\alpha} w_\beta + v^\beta w_{\beta;\alpha}. \quad (19)$$

The result is that $v_{\alpha;\beta} := v_{\alpha,\beta} - v_\gamma \Gamma_{\alpha\beta}^\gamma$, which is consistent with the notion of using the metric as a raising / lowering operator (*i.e.*, $v_{\alpha;\beta} = g_{\alpha\gamma} v^\gamma_{;\beta}$). In coordinate free notation, this is equivalent to

$$(\nabla_{\vec{y}} v)(\vec{w}) := \nabla_{\vec{y}} [v(\vec{w})] - v(\nabla_{\vec{y}} \vec{w}). \quad (20)$$

- For a general (r, s) -valent tensor $T : (\otimes^r T\mathcal{S}_t) \otimes (\otimes^s T^*\mathcal{S}_t) \rightarrow \mathbb{R}$, acting on r vectors $\vec{w}_1, \dots, \vec{w}_r \in T\mathcal{S}_t$ and s 1-forms $p_1, \dots, p_s \in T^*\mathcal{S}_t$, the covariant derivative is given by the following formula:

$$\begin{aligned} (\nabla_{\vec{y}} T)(\vec{v}_1, \dots, \vec{v}_r, p_1, \dots, p_s) := & \vec{y} [T(\vec{v}_1, \dots, \vec{v}_r, p_1, \dots, p_s)] \\ & - T(\nabla_{\vec{y}} \vec{v}_1, \dots, \vec{v}_r, p_1, \dots, p_s) - \dots - T(\vec{v}_1, \dots, \nabla_{\vec{y}} \vec{v}_r, p_1, \dots, p_s) \\ & - T(\vec{v}_1, \dots, \vec{v}_r, \nabla_{\vec{y}} p_1, \dots, p_s) - \dots - T(\vec{v}_1, \dots, \vec{v}_r, p_1, \dots, \nabla_{\vec{y}} p_s). \end{aligned} \quad (21)$$

In component form, this is equivalent to

$$\begin{aligned} \nabla_{\vec{y}} T := & \left(y^\gamma T^{\beta_1 \dots \beta_s}_{\alpha_1 \dots \alpha_r, \gamma} - T^{\beta_1 \dots \beta_s}_{\delta \dots \alpha_r} \Gamma_{\alpha_1 \gamma}^\delta y^\gamma - \dots - T^{\beta_1 \dots \beta_s}_{\alpha_1 \dots \delta} \Gamma_{\alpha_r \gamma}^\delta y^\gamma \right. \\ & \left. + T^{\delta \dots \beta_s}_{\alpha_1 \dots \alpha_r} \Gamma_{\delta \gamma}^{\beta_1} y^\gamma + \dots + T^{\beta_1 \dots \delta}_{\alpha_1 \dots \alpha_r} \Gamma_{\delta \gamma}^{\beta_s} y^\gamma \right) du^{\alpha_1} \otimes \dots \otimes du^{\alpha_r} \otimes \vec{e}_{\beta_1} \otimes \dots \otimes \vec{e}_{\beta_s}. \end{aligned} \quad (22)$$

D. Second fundamental form, Gauss and Weingarten equations

Consider the derivative

$$\frac{\partial \hat{\mathbf{n}}}{\partial u^\alpha} =: \hat{\mathbf{n}}_{,\alpha}, \quad (23)$$

i.e., the rate-of-change in the unit normal to \mathcal{S}_t along u^α , expressed as a vector in \mathbb{R}^3 . Since $\hat{\mathbf{n}}$ is a unit vector, the result must still be tangent to \mathcal{S}_t and therefore

$$\hat{\mathbf{n}}_{,\alpha} = -b^\beta_{\alpha} \mathbf{R}_{t*}(\vec{e}_\beta) = -b^\beta_{\alpha} \mathbf{R}_{,\beta}, \quad (24)$$

which is known as the Weingarten equation (the assignment of a minus sign being convention). Given the right-hand side, we can use the coefficients from the above to construct a linear map $b : T_u \mathbb{R}^2 \rightarrow T_u \mathbb{R}^2$ by writing $\vec{b}(\vec{v}) = -v^\beta \vec{e}_\alpha b^\alpha_{\beta}$, for arbitrary \vec{v} . Similarly, there is a natural bilinear form II, known as the *second fundamental form*, that can be associated with such a map, whose action is given by

$$\text{II}(\vec{v}, \vec{w}) = \langle \vec{v}, \vec{b}(\vec{w}) \rangle = v^\gamma w^\beta \langle \vec{e}_\gamma, -b^\alpha_{\beta} \vec{e}_\alpha \rangle. \quad (25)$$

That is

$$\text{II} = -[\mathbf{R}_{t*}(\vec{e}_\alpha) \cdot \hat{\mathbf{n}}_{,\beta}] du^\alpha \otimes du^\beta = -[\mathbf{R}_{,\alpha} \cdot \hat{\mathbf{n}}_{,\beta}] du^\alpha \otimes du^\beta = b_{\alpha\beta} du^\alpha \otimes du^\beta, \quad (26)$$

where $b_{\alpha\beta} = g_{\alpha\gamma} b^\gamma_{\beta}$. Notice that since $\partial[\mathbf{R}_{,\alpha} \cdot \hat{\mathbf{n}}]/\partial u^\beta = 0$, we have $b_{\alpha\beta} = (\partial \mathbf{R}_{,\alpha}/\partial u^\beta) \cdot \hat{\mathbf{n}} = \mathbf{R}_{,\alpha\beta} \cdot \hat{\mathbf{n}}$. More generally, the derivative of basis vectors \vec{e}_α with respect to some coordinate u^β on \mathcal{S}_t can be decomposed into tangent and normal parts.

$$\mathbf{R}_{,\alpha\beta} = \Gamma_{\alpha\beta}^\gamma \mathbf{R}_{,\gamma} + b_{\alpha\beta} \hat{\mathbf{n}}, \quad (27)$$

which is known as Gauss’ equation.

E. Curvature

At a given point u , each unit vector \hat{y} corresponds to a unique curve \mathcal{C} on \mathcal{S}_t that also lies in the plane \mathcal{P}_t spanned by \hat{n} and $\mathbf{R}_{t*}(\hat{y}) = y^\alpha \mathbf{R}_{,\alpha}$. The action of the second fundamental form on a given \hat{y} results in the *normal curvature* $c_{\hat{y}}^{(n)}$ of \mathcal{S}_t in the direction of $y^\alpha \mathbf{R}_{,\alpha}$ (*i.e.*, the curvature of \mathcal{C} in \mathcal{P}_t). We write,

$$\Pi(\hat{y}, \hat{y}) = \pm c_{\hat{y}}^{(n)}, \quad (28)$$

where “+” indicates whether \mathcal{C} is curving towards the unit normal, and vice-versa for “-”. Since the normal curvature will change dependent on which direction \hat{y} is chosen, we define the principal directions:

$$\hat{y}_1(p) = \arg \max_{\hat{y} \in T_p \mathbb{R}^2} \Pi(\hat{y}, \hat{y}), \quad \text{and} \quad \hat{y}_2(p) = \arg \min_{\hat{y} \in T_p \mathbb{R}^2} \Pi(\hat{y}, \hat{y}). \quad (29)$$

The principal curvatures are then given by

$$c_\alpha(p) = \Pi(\hat{y}_\alpha, \hat{y}_\alpha), \quad \forall \alpha = 1, 2. \quad (30)$$

It can be shown that the c_α are eigenvalues of the linear operator \vec{b} from §X D. That is,

$$\vec{b}(\hat{y}_\alpha) = c_\alpha \hat{y}_\alpha, \quad (31)$$

where if $c_1 \neq c_2$, the principal directions are orthogonal. We may now define two different types of local curvature of \mathcal{S}_t : the *mean curvature*

$$H := \frac{1}{2} \text{Tr} b^\alpha_\beta = \frac{1}{2} \text{Tr}_g \Pi = \frac{c_1 + c_2}{2}, \quad (32)$$

and the *Gaussian curvature*

$$K := \det b^\alpha_\beta = \frac{\det b_{\alpha\beta}}{\det g_{\alpha\beta}} = c_1 c_2. \quad (33)$$

F. Interior product and trace

The action of a differential form on a vector is essentially a contraction. (To see this, consider a 1-form v acting on a vector \vec{w} : $v(\vec{w}) = v^\alpha w_\alpha$). For forms of higher degree, if $p^{(r)}$ is an r -form and \vec{v} a vector, then $i_{\vec{v}} p^{(r)}$ is an $(r-1)$ -form—*i.e.*, the *interior product* of $p^{(r)}$ with respect to \vec{v} . If, $\vec{w}_1, \vec{w}_2, \dots, \vec{w}_r$ are r arbitrary vectors, then

$$i_{\vec{v}} p^{(r)}(\vec{w}_1, \dots, \vec{w}_{r-1}) = p^{(r)}(\vec{v}, \vec{w}_1, \dots, \vec{w}_{r-1}). \quad (34)$$

The interior product $i_{\vec{v}} : \bigwedge^k T^* \mathcal{S}_t \rightarrow \bigwedge^{k-1} T^* \mathcal{S}_t$ is an *antiderivation*, which means that its action over the wedge product is given by

$$i_{\vec{v}} [p^{(r)} \wedge q^{(s)}] = [i_{\vec{v}} p^{(r)}] \wedge q^{(s)} + (-1)^r p^{(r)} \wedge [i_{\vec{v}} q^{(s)}]. \quad (35)$$

The interior product contracts a form with a vector, reducing the degree of the form. For contractions between *pairs* of coefficients of a form, the notion of a generalised trace $\text{Tr}_g^{(a,b)}$ is needed. Here, the subscript g indicates a trace *through* the metric (*i.e.*, to ensure that contractions only take place between indices of different types) whilst the integers a and b indicate the indices over which to contract. For example, the trace of r -form $p^{(r)}$ gives a $(r-2)$ -form:

$$\text{Tr}_g^{(1,3)} [p^{(r)}] (\vec{w}_1, \dots, \vec{w}_{r-2}) = p^{(r)} (\vec{e}_i, \vec{w}_1, \vec{e}_j, \dots, \vec{w}_{r-2}) g^{ij}. \quad (36)$$

G. Exterior derivative

The exterior derivative $d : \bigwedge^k T^* \mathcal{S}_t \rightarrow \bigwedge^{k+1} T^* \mathcal{S}_t$ takes k -forms and returns $(k+1)$ -forms. In our setup:

- If φ is a 0-form, or function, then

$$d\varphi = \left(\frac{\partial\varphi}{\partial u^1} \right) du^1 + \left(\frac{\partial\varphi}{\partial u^2} \right) du^2. \quad (37)$$

By the identification of vectors with 1-forms (see §X A) $d\varphi$ is dual to the gradient of φ . That is, $d\varphi(\vec{v}) = \langle \nabla\varphi, \vec{v} \rangle$ for all vectors \vec{v} , where

$$\nabla\varphi := g^{\alpha\beta} \frac{\partial\varphi}{\partial u^\alpha} \vec{e}_\beta, \quad (38)$$

is just the gradient operator induced by the embedding.

- If $\omega = \omega_\alpha du^\alpha$ is a 1-form, then

$$d\omega = \left[\left(\frac{\partial\omega_2}{\partial u^1} \right) - \left(\frac{\partial\omega_1}{\partial u^2} \right) \right] du^1 \wedge du^2. \quad (39)$$

Repeated application always yields zero— *i.e.*, $ddp = d^2p = 0$ for an arbitrary exterior form p . Also, the action of d is an *antiderivation*. That is,

$$d \left[p^{(r)} \wedge q^{(s)} \right] = dp^{(r)} \wedge q^{(s)} + (-1)^r p^{(r)} \wedge dq^{(s)}, \quad (40)$$

where $p^{(r)}$ and $q^{(s)}$ are exterior forms of degree r and s , respectively.

XI. MORPHOLOGY

We assume that the surface of connected Apical faces may be approximated by the manifold \mathcal{S}_t . For \mathcal{S}_t to change in time, each point $\mathbf{R}(u, t) =: \mathbf{R}_t(u)$ must move with a velocity $\mathbf{v}(u, t) := \partial_t \mathbf{R}(u, t) \in T_{\mathbf{R}(u, t)} \mathbb{R}^3$. In the following, we show how the local structure of \mathcal{S}_t changes as points move under the action of \mathbf{v} .

A. Rate-of-change of the metric in time

We wish to calculate the partial derivative $\partial_t g_{\alpha\beta}$. Applying the product rule, we have

$$\partial_t g_{\alpha\beta} = (\partial_t \mathbf{R}_{,\alpha}) \cdot \mathbf{R}_{,\beta} + \mathbf{R}_{,\alpha} \cdot (\partial_t \mathbf{R}_{,\beta}). \quad (41)$$

Here, since the coordinates u do not depend on time, the partial derivatives $\partial/\partial t$ and $\partial/\partial u^\alpha$ commute, giving

$$\partial_t g_{\alpha\beta} = \mathbf{v}_{,\alpha} \cdot \mathbf{R}_{,\beta} + \mathbf{R}_{,\alpha} \cdot \mathbf{v}_{,\beta}. \quad (42)$$

Decomposing \mathbf{v} into parts that are tangential- and normal-to \mathcal{S}_t , we have $\mathbf{v} = v^\alpha \mathbf{R}_{,\alpha} + v^{(n)} \hat{\mathbf{n}}$, which can be substituted into $\mathbf{v}_{,\alpha}$ to give

$$\mathbf{v}_{,\alpha} = v^\beta{}_{,\alpha} \mathbf{R}_{,\beta} + v^\beta \mathbf{R}_{,\beta\alpha} + v^{(n)}{}_{,\alpha} \hat{\mathbf{n}} + v^{(n)} \hat{\mathbf{n}}_{,\alpha}. \quad (43)$$

Imposing the Gauss (27) and Wiegarten (24) equations, we see that

$$\mathbf{v}_{,\alpha} = \left(v^\beta{}_{,\alpha} + v^\gamma \Gamma_{\alpha\gamma}^\beta - v^{(n)} b_\alpha{}^\beta \right) \mathbf{R}_{,\beta} + \left(b_{\alpha\beta} v^\beta + v^{(n)}{}_{,\alpha} \right) \hat{\mathbf{n}}. \quad (44)$$

Substituting (44) into (42), the raising and lowering properties of the metric and the relation $g_{\alpha\beta,\gamma} = \Gamma_{\alpha\gamma}^\kappa g_{\kappa\beta} + \Gamma_{\beta\gamma}^\kappa g_{\kappa\alpha}$ may be used to show that

$$\partial_t g_{\alpha\beta} = v_{\alpha;\beta} + v_{\beta;\alpha} - 2 v^{(n)} b_{\alpha\beta}, \quad (45)$$

where a subscript colon “;” is used to denote the components of the covariant derivative (see §X C).

B. Rate-of-change of local area in time

The local area at a point u on \mathcal{S}_t is just given by \sqrt{g} , where

$$g := \det g_{\alpha\beta} = \frac{1}{2} \varepsilon^{\alpha\mu} \varepsilon^{\beta\nu} g_{\alpha\beta} g_{\mu\nu}, \quad (46)$$

for 2×2 symmetric matrices. Here, $\varepsilon^{\alpha\beta}$ is a two-dimensional antisymmetric Levi-Civita symbol (a rank-(0,2) tensor density of weight +1). Taking the partial derivative with respect to time yields

$$\partial_t \sqrt{g} = \frac{1}{2\sqrt{g}} \varepsilon^{\alpha\mu} \varepsilon^{\beta\nu} g_{\alpha\beta} (\partial_t g_{\mu\nu}) = \frac{1}{2\sqrt{g}} \varepsilon^{\alpha\mu} \varepsilon^{\beta\nu} g_{\alpha\beta} (v_{\alpha;\beta} + v_{\beta;\alpha} - 2v^{(n)} b_{\alpha\beta}) \quad (47)$$

where (45) has been used. Using the fact that

$$g^{\alpha\beta} = \frac{1}{g} \varepsilon^{\alpha\mu} \varepsilon^{\beta\nu} g_{\mu\nu}, \quad (48)$$

gives the result

$$\partial_t \sqrt{g} = \sqrt{g} (v^\alpha{}_{;\alpha} - v^{(n)} 2H). \quad (49)$$

C. Relationship to conservation of cell number density

Dividing (49) by \sqrt{g} we see that

$$\partial_t \log \left(\frac{\sqrt{g}}{\sqrt{g_0}} \right) = v^\alpha{}_{;\alpha} - v^{(n)} 2H, \quad (50)$$

where a subscript is used for notational convenience [*i.e.*, $g_0(u) = g(u, 0)$]. However, since there is no cell division or death, the tissue is of fixed connectivity and cannot flow relative to u , implying $\rho_0 \sqrt{g_0} = \rho \sqrt{g}$, where $\rho(u, t)$ is the local number density (per unit area) of cells. As a result

$$\log \left(\frac{\sqrt{g}}{\sqrt{g_0}} \right) = -\log \left(\frac{\rho}{\rho_0} \right), \quad (51)$$

and hence

$$\partial_t \rho + \rho v^\alpha{}_{;\alpha} - \rho v^{(n)} 2H = 0. \quad (52)$$

This is precisely the equation for a conserved scalar field associated with a moving manifold, but without the standard convective term $v^\alpha \rho_{;\alpha}$, which does not appear because, by construction, cells cannot flow relative to the internal coordinate u . [Note that this can also be seen as a consequence of the fact that \sqrt{g} is a rank-0 tensor density of weight +1, and therefore its covariant derivative vanishes, *i.e.*, $(\sqrt{g})_{;\alpha} = 0$].

D. Rate-of-change of the coefficients of the second fundamental form in time

In a similar way as for the metric, consider calculating $\partial_t b_{\alpha\beta}$, where $b_{\alpha\beta} = \mathbf{R}_{,\alpha\beta} \cdot \hat{\mathbf{n}}$ are the coefficients of the second fundamental form. Using the product rule, we have

$$\partial_t b_{\alpha\beta} = (\partial_t \mathbf{R}_{,\alpha\beta}) \cdot \hat{\mathbf{n}} + \mathbf{R}_{,\alpha\beta} \cdot (\partial_t \hat{\mathbf{n}}), \quad (53)$$

where we consider each of the two terms on the right-hand side in turn. For the first term, by commuting time and space derivatives as before, we see that $\partial_t \mathbf{R}_{,\alpha\beta} = \mathbf{v}_{,\alpha\beta}$. Taking the partial derivative $\partial/\partial u^\beta$ of (43), applying Gauss' equation (27), and retaining only components in the $\hat{\mathbf{n}}$ direction, gives

$$(\partial_t \mathbf{R}_{,\alpha\beta}) \cdot \hat{\mathbf{n}} = \mathbf{v}_{,\alpha\beta} \cdot \hat{\mathbf{n}} = (v^\gamma{}_{;\alpha} - v^{(n)} b_\alpha{}^\gamma) b_{\gamma\beta} + (b_{\alpha\gamma} v^\gamma)_{,\beta} + v_{,\alpha\beta}^{(n)}. \quad (54)$$

For the second term, it is necessary to understand $\partial_t \hat{\mathbf{n}}$. Here, since $\partial_t |\hat{\mathbf{n}}|^2 = 0$, we see that $\hat{\mathbf{n}} \cdot (\partial_t \hat{\mathbf{n}}) = 0$, *i.e.*, $\partial_t \hat{\mathbf{n}}$ has no normal component. Moreover, since $\mathbf{R}_{,\alpha} \cdot \hat{\mathbf{n}} = 0$ then $\mathbf{v}_{,\alpha} \cdot \hat{\mathbf{n}} = \mathbf{R}_{,\alpha} \cdot (\partial_t \hat{\mathbf{n}})$, which implies

$$\partial_t \hat{\mathbf{n}} = -v^\beta b_\beta^\alpha \mathbf{R}_{,\alpha} - v_{,\alpha}^{(n)} g^{\alpha\beta} \mathbf{R}_{,\beta}. \quad (55)$$

Substituting into $\mathbf{R}_{,\alpha\beta} \cdot (\partial_t \hat{\mathbf{n}})$ and once again using Gauss' equation (27), gives

$$\mathbf{R}_{,\alpha\beta} \cdot (\partial_t \hat{\mathbf{n}}) = \Gamma_{\alpha\beta}^\gamma v^\kappa b_{\kappa\gamma} - \Gamma_{\alpha\beta}^\gamma v_{,\gamma}^{(n)}. \quad (56)$$

The expressions (54) and (56) can be substituted into (53) with the following results:

$$\partial_t b_{\alpha\beta} = b_{\gamma\beta} v^\gamma_{;\alpha} + (b_{\alpha\beta} v^\beta)_{;\alpha} + v_{,\alpha;\beta}^{(n)} - v^{(n)} b_{\alpha\gamma} b_{\gamma\beta} \quad (57)$$

$$= b_{\gamma\beta} v^\gamma_{;\alpha} + b_{\alpha\gamma} v^\gamma_{;\beta} + v^\gamma b_{\alpha\beta;\gamma} + v_{,\alpha;\beta}^{(n)} - v^{(n)} (2H b_{\alpha\beta} - K g_{\alpha\beta}). \quad (58)$$

Here, the last line uses the relation $b_{\alpha\gamma} b_{\gamma\beta} = 2H b_{\alpha\beta} - K g_{\alpha\beta}$, and the fact that the coefficients of the covariant derivative of a rank-(2,0) tensor (§XC) are

$$b_{\alpha\beta;\gamma} = b_{\alpha\beta,\gamma} - b_{\alpha\kappa} \Gamma_{\beta\gamma}^\kappa - b_{\kappa\beta} \Gamma_{\alpha\gamma}^\kappa. \quad (59)$$

E. Rate-of-change of mean curvature in time

Using the above results, it is possible to calculate the rate of change of mean curvature (32) in time. We have

$$\partial_t H = \frac{1}{2} (\partial_t b_{\alpha\beta}) g^{\alpha\beta} + \frac{1}{2} b_{\alpha\beta} (\partial_t g_{\alpha\beta}) = \frac{1}{2} (\partial_t b_{\alpha\beta}) g^{\alpha\beta} - \frac{1}{2} b^{\alpha\beta} (\partial_t g_{\alpha\beta}), \quad (60)$$

where, in the last equality we use the fact that $\partial_t \delta_\beta^\alpha = 0$, which implies

$$\partial_t g^{\alpha\beta} = -g^{\alpha\mu} g^{\beta\nu} \partial_t (g_{\mu\nu}). \quad (61)$$

Substituting for the results (45), (58) and using $b_{\alpha\beta} b^{\alpha\beta} = 4H^2 - 2K$, gives

$$\partial_t H = v^\alpha H_{,\alpha} + \frac{1}{2} \Delta v^{(n)} + v^{(n)} (2H^2 - K), \quad (62)$$

where $\Delta := \partial_\alpha (\sqrt{g} g^{\alpha\beta} \partial_\beta) / \sqrt{g}$ is the Laplace-Beltrami operator.

XII. MECHANICAL RESPONSE

The mechanical response of the tissue under deformation is assumed to be elastic-like, with restoring forces that are linear in strain corresponding to each of the apical, basal and lateral cell faces.

A. Apical

Consider first the Apical manifold \mathcal{S}_t . Using the theory of finite strains, we consider the difference between two configurations: an unstrained state \mathcal{S}^\dagger and the state at time t , \mathcal{S}_t . To do this, we introduce $\phi : \mathbb{R}^2 \rightarrow \mathbb{R}^3$, the embedding function for the unstrained state \mathcal{S}^\dagger [*i.e.*, $\phi(u, t) = \mathbf{R}^\dagger(u, t)$ and $\phi_*(\vec{e}_\alpha) = \mathbf{R}_{,\alpha}^\dagger$]. The coefficients of the pullback (to \mathbb{R}^2) of the Green-Lagrange strain form are then

$$\epsilon_{\alpha\beta} = [(\mathbf{R}_t^* - \phi^*) \mathbb{I}] (\vec{e}_\alpha, \vec{e}_\beta) = \mathbf{R}_{,\alpha} \cdot \mathbf{R}_{,\beta} - \mathbf{R}_{,\alpha}^\dagger \cdot \mathbf{R}_{,\beta}^\dagger = g_{\alpha\beta} - g_{\alpha\beta}^\dagger, \quad (63)$$

where $\mathbb{I} = \delta_{ij} dx^i \otimes dx^j$ is just the first fundamental form of three-dimensional Euclidean space, and $g_{\alpha\beta}^\dagger$ is the metric of the unstrained state.

We then construct an effective free energy density (per unit area) for the Apical faces that is quadratic in the coefficients $\epsilon_{\alpha\beta}$. The most general way is to contract two copies of (63) with a rank-(0,4) elasticity tensor *i.e.*,

$C^{\alpha\beta\gamma\delta} \epsilon_{\alpha\beta} \epsilon_{\gamma\delta}$. For our treatment, it suffices to follow the usual decomposition of C between trace and symmetric-traceless parts:

$$C^{\alpha\beta\gamma\delta} = \mu_A \left(g^{\alpha\gamma} g^{\beta\delta} - \frac{1}{2} g^{\alpha\beta} g^{\gamma\delta} \right) + \left(\lambda_A + \frac{\mu_A}{2} \right) g^{\alpha\beta} g^{\gamma\delta}, \quad (64)$$

such that μ_A and λ_A resemble the first and second Lamé coefficients of the Apical surface, respectively. (Note that, in principle, the values of μ_A and λ_A can rely on the concentrations of wide variety of molecules, from passive cross-linkers to cell-cell adhesions *etc.*).

B. Basal

The surface of connected Basal faces is also assumed to be approximated by a smooth Riemannian manifold, \mathcal{S}_t^B . In a ‘‘thin film’’ approximation, we make the assumption that \mathcal{S}_t^B is given by taking a normal projection from \mathcal{S}_t , such that $\mathbf{R}_B(u, t) = \mathbf{R}(u, t) - \ell(u, t) \hat{\mathbf{n}}(u, t)$, where ℓ is the tissue thickness. The metric of the Basal manifold can then be written in terms of the metric of the Apical manifold via power series expansion in $|\ell H| \ll 1$, *e.g.*,

$$g_{\alpha\beta}^B = g_{\alpha\beta} + 2\ell b_{\alpha\beta} + \ell^2 (2H b_{\alpha\beta} - K g_{\alpha\beta}) + \ell_{,\alpha} \ell_{,\beta} + O(\ell^3), \quad (65)$$

and

$$g_B^{\alpha\beta} = g^{\alpha\beta} - 2\ell b^{\alpha\beta} + 3\ell^2 (2H b_{\alpha\beta} - K g_{\alpha\beta}) - \ell_{,\alpha} \ell_{,\beta} + O(\ell^3). \quad (66)$$

As explained in the main manuscript, we neglect the final terms in these expansions, making the assumption that $|\ell_{,\alpha}| \ll \ell |H|$. The effective free-energy density (per unit area) of the basal surface is then $C_B^{\alpha\beta\gamma\delta} \epsilon_{\alpha\beta}^B \epsilon_{\gamma\delta}^B$, where the coefficients of the basal Green-Lagrange strain form (§XII A) are

$$\epsilon_{\alpha\beta}^B = g_{\alpha\beta}^B - g_{\alpha\beta}^{\dagger B}, \quad (67)$$

and

$$C_B^{\alpha\beta\gamma\delta} = \mu_B \left(g_B^{\alpha\gamma} g_B^{\beta\delta} - \frac{1}{2} g_B^{\alpha\beta} g_B^{\gamma\delta} \right) + \left(\lambda_B + \frac{\mu_B}{2} \right) g_B^{\alpha\beta} g_B^{\gamma\delta}, \quad (68)$$

such that μ_B and λ_B may differ from μ_A and λ_A .

C. Lateral

The lateral cell walls are assumed to have a rest length ℓ^\dagger and therefore have a contribution to the effective free energy of the form $\kappa (\ell - \ell^\dagger)^2$, where κ has the dimensions of an elastic modulus. Some vertex models have included an interfacial contribution, proportional to the total area of lateral faces. However, there is scant experimental evidence that such terms contribute at to energetics at lowest order, therefore they are omitted for simplicity.

D. Volume constraint

Summing contributions from apical, basal and lateral faces, the total effective free-energy of the tissue is given by

$$\mathcal{F} = \int_{\mathbb{R}^2} F(\mathbf{R}_{,\alpha}, \mathbf{R}_{,\alpha\beta}, \ell) \text{vol}^2. \quad (69)$$

Since the density of cortical actin associated with the lateral faces is lower than that of either the apical or basal faces, we assume that the relaxation time of ℓ is significantly faster than $g_{\alpha\beta}$, and hence we impose $\delta\mathcal{F}/\delta\ell = 0$. The minimisation must be performed under the constraint that cells do not change their volume. Once again appealing to the thin film approximation, the area of lateral slice of tissue, projected a distance z in the $-\hat{\mathbf{n}}$ direction from \mathcal{S}_t is $\sqrt{g_z} = \sqrt{g} (1 + 2zH) + O(z^2)$, and therefore

$$V = \int_0^\ell dz \sqrt{g_z} = \ell \sqrt{g} (1 + \ell H) + O(\ell^3), \quad (70)$$

where V is time-independent.

E. Variation of the effective free-energy

Using the aforementioned procedure to eliminate ℓ results in an effective free-energy functional whose dynamical degrees of freedom are purely geometrical, *i.e.*,

$$\mathcal{F} = \int_{\mathbb{R}^2} F(\mathbf{R}_{,\alpha}, \mathbf{R}_{,\alpha\beta}) \text{vol}^2, \quad (71)$$

where $\text{vol}^2 = \sqrt{g} du^1 \wedge du^2$ is the induced volume form on \mathbb{R}^2 . We wish to calculate the functional derivative of \mathcal{F} with respect to variations in the embedding $\mathbf{R}(u, t)$. That is, the response of the system (*i.e.*, the forces per unit area) to deformations of \mathcal{S}_t .

Formally, we consider the variation $\delta\mathcal{F}$ arising due to changes to \mathcal{S}_t of the form $\mathbf{R} + \epsilon\boldsymbol{\eta}$, where ϵ is a small dimensionless parameter. We write

$$\delta\mathcal{F} = \epsilon \left. \frac{d\mathcal{F}}{d\epsilon} \right|_{\epsilon=0} = \epsilon \int_{\mathbb{R}^2} (\boldsymbol{\eta}_{,\alpha} \cdot \mathbf{A}^\alpha + \boldsymbol{\eta}_{;\alpha\beta} \cdot \mathbf{B}^{\alpha\beta}) \text{vol}^2, \quad (72)$$

where

$$\mathbf{A}^\alpha := \frac{1}{\sqrt{g}} \frac{\partial(\sqrt{g}F)}{\partial \mathbf{R}_{,\alpha}} = \pi^{\alpha\beta} \mathbf{R}_{,\beta}, \quad (73)$$

and

$$\mathbf{B}^{\alpha\beta} := \frac{\partial F}{\partial \mathbf{R}_{,\alpha\beta}} = \psi^{\alpha\beta} \hat{\mathbf{n}}, \quad (74)$$

By using the chain rule and the fact that $\partial g / \partial g_{\alpha\beta} = g g^{\alpha\beta}$ [see (46) and (48)], it can be shown that

$$\pi^{\alpha\beta} = \frac{1}{\sqrt{g}} \frac{\partial(\sqrt{g}F)}{\partial g_{\alpha\beta}} = \frac{F g^{\alpha\beta}}{2} + \frac{\partial F}{\partial g_{\alpha\beta}}. \quad (75)$$

Similarly, from Gauss' equation (27) and orthogonality ($\mathbf{R}_{,\mu} \cdot \hat{\mathbf{n}} = 0$) we have

$$\psi^{\alpha\beta} = \frac{\partial F}{\partial b_{\alpha\beta}}. \quad (76)$$

We proceed by integrating by parts which, in the language of differential geometry, is just an application of Stokes theorem [18]. For the first term on the right-hand side of (72) let ω be a 1-form, such that

$$\omega = \boldsymbol{\eta} \cdot \mathbf{R}_{,\alpha} \pi^{\alpha\beta} i_{\vec{e}_\beta} \text{vol}^2, \quad (77)$$

where i represents the interior product (§XF). Applying the exterior derivative (§XG), we have

$$d\omega = \boldsymbol{\eta}_{,\beta} \cdot \mathbf{R}_{,\alpha} \pi^{\alpha\beta} \text{vol}^2 + \boldsymbol{\eta} \cdot (\mathbf{R}_{,\alpha} \pi^{\alpha\beta}_{;\beta} + \hat{\mathbf{n}} \pi^{\alpha\beta} b_{\alpha\beta}) \text{vol}^2, \quad (78)$$

where a subscript colon “;” is used according to (21). Under the usual assumption that $\boldsymbol{\eta}(u, t) \rightarrow 0$ as $|u| \rightarrow \infty$, Stokes theorem then gives

$$\int_{\mathbb{R}^2} \boldsymbol{\eta}_{,\beta} \cdot \mathbf{R}_{,\alpha} \pi^{\alpha\beta} \text{vol}^2 = - \int_{\mathbb{R}^2} \boldsymbol{\eta} \cdot (\mathbf{R}_{,\alpha} \pi^{\alpha\beta}_{;\beta} + \hat{\mathbf{n}} \pi^{\alpha\beta} b_{\alpha\beta}) \text{vol}^2. \quad (79)$$

For the second term on the right-hand side of (72), consider the 1-form

$$\xi = \boldsymbol{\eta}_{,\alpha} \cdot \hat{\mathbf{n}} \psi^{\alpha\beta} i_{\vec{e}_\beta} \text{vol}^2, \quad (80)$$

which, via §XF, implies

$$d\xi = \boldsymbol{\eta}_{,\alpha\beta} \cdot \hat{\mathbf{n}} \psi^{\alpha\beta} \text{vol}^2 + \boldsymbol{\eta}_{,\alpha} \cdot [\hat{\mathbf{n}} (\psi^{\alpha\beta}_{;\beta} - \psi^{\mu\nu} \Gamma_{\mu\nu}^\alpha) - \mathbf{R}_{,\gamma} b^\gamma_\beta \psi^{\alpha\beta}] \text{vol}^2, \quad (81)$$

and therefore, under the assumption that $\boldsymbol{\eta}_{,\alpha}(u, t) \rightarrow 0$ as $|u| \rightarrow \infty$, applying Stokes theorem gives the result

$$\int_{\mathbb{R}^2} \boldsymbol{\eta}_{,\alpha\beta} \cdot \hat{\mathbf{n}} \psi^{\alpha\beta} \text{vol}^2 = \int_{\mathbb{R}^2} \boldsymbol{\eta}_{,\alpha} \cdot (\mathbf{R}_{,\gamma} b^\gamma_\beta \psi^{\alpha\beta} - \hat{\mathbf{n}} \psi^{\alpha\beta}_{;\beta}) \text{vol}^2, \quad (82)$$

where we have used the fact that $\boldsymbol{\eta}_{;\alpha;\beta} = \boldsymbol{\eta}_{,\alpha\beta} - \boldsymbol{\eta}_{,\gamma} \Gamma_{\alpha\beta}^{\gamma}$. The final step is to apply Stokes theorem to the right-hand side of (82). To this end, consider the 1-form

$$\zeta = \boldsymbol{\eta} \cdot (\mathbf{R}_{,\gamma} b^{\gamma}_{\beta} \psi^{\alpha\beta} - \hat{\mathbf{n}} \psi^{\alpha\beta}_{;\beta}) i_{\vec{e}_{\alpha}} \text{vol}^2, \quad (83)$$

which, via §XF, implies

$$d\zeta = \boldsymbol{\eta}_{,\alpha} \cdot (\mathbf{R}_{,\gamma} b^{\gamma}_{\beta} \psi^{\alpha\beta} - \hat{\mathbf{n}} \psi^{\alpha\beta}_{;\beta}) \text{vol}^2 + \boldsymbol{\eta} \cdot \left[\mathbf{R}_{,\alpha} (b^{\alpha}_{\gamma} \psi^{\gamma\beta})_{;\beta} + \hat{\mathbf{n}} b^{\alpha}_{\gamma} \psi^{\gamma\beta} b_{\alpha\beta} + \mathbf{R}_{,\gamma} b^{\gamma}_{\alpha} \psi^{\alpha\beta}_{;\beta} - \hat{\mathbf{n}} \psi^{\alpha\beta}_{;\alpha\beta} \right] \text{vol}^2. \quad (84)$$

After a final application of Stokes Theorem, the result can be combined with (79) and (82) to identify the functional derivative via

$$\delta\mathcal{F} = \epsilon \int_{\mathbb{R}^2} \boldsymbol{\eta} \cdot \left(\frac{\delta\mathcal{F}}{\delta\mathbf{R}} \right) \text{vol}^2, \quad (85)$$

which gives

$$\frac{\delta\mathcal{F}}{\delta\mathbf{R}} = \left[-\pi^{\alpha\beta}_{;\beta} - (b^{\alpha}_{\gamma} \psi^{\gamma\beta})_{;\beta} - b^{\alpha}_{\gamma} \psi^{\gamma\beta}_{;\beta} \right] \mathbf{R}_{,\alpha} + \left[-\pi^{\alpha\beta} b_{\alpha\beta} - \psi^{\alpha\beta} (2H b_{\alpha\beta} - K g_{\alpha\beta}) + \psi^{\alpha\beta}_{;\alpha\beta} \right] \hat{\mathbf{n}}. \quad (86)$$

XIII. DISSIPATION

We may estimate the relative rates of energy dissipation that can be attributed to the tissue and the embedding fluid, respectively, during gastrulation. The former arises not from relative movements of cells, but due to viscous shear of the enclosed cytosol as cells are deformed. The latter arises due to viscous shear of the yolk.

We imagine the embryo as a sphere, parameterised in the usual spherical coordinates: radius R , azimuthal angle ϕ , and polar angle θ . We consider a surface flow $\mathbf{v} = V \sin\theta \hat{\boldsymbol{\phi}}$. In the bulk, assuming a no-slip boundary condition, geometric constraints impose a characteristic velocity gradient V/R . An order of magnitude estimate of the rate of energy dissipation $\partial_t E_{\text{bulk}}$ is therefore given by

$$\partial_t E_{\text{bulk}} \sim \eta_{\text{bulk}} \left(\frac{V}{R} \right)^2 \frac{4}{3} \pi R^3. \quad (87)$$

By contrast, on the surface, the characteristic velocity gradient is $2V/\pi R$. Implying

$$\partial_t E_{\text{surf}} \sim \eta_{\text{surf}} \left(\frac{2V}{\pi R} \right)^2 4\pi R^2 \ell, \quad (88)$$

where ℓ is the thickness of the epithelium. As a result

$$\frac{\partial_t E_{\text{bulk}}}{\partial_t E_{\text{surf}}} \sim \frac{\eta_{\text{bulk}}}{\eta_{\text{surf}}} \frac{R}{\ell} \frac{\pi^2}{12}. \quad (89)$$

Assuming representative values $R = 200 \mu\text{m}$ and $\ell = 10 \mu\text{m}$ [5], we may also use the fact that the meso-scale viscosity of cellular cytosol is approximately 1 Pa s [15], as is the viscosity of embryonic yolk [16]. For *Drosophila*, therefore, this gives

$$\frac{\partial_t E_{\text{bulk}}}{\partial_t E_{\text{surf}}} \sim 2\pi^2, \quad (90)$$

implying that the dissipative contribution of the yolk is at least an order of magnitude greater than that of the epithelium.

XIV. ACTIVE CONTRACTILITY

An active contractile stress $\boldsymbol{\sigma} = \sigma^{\alpha\beta} \mathbf{R}_{,\alpha} \otimes \mathbf{R}_{,\beta}$ acts in the tangent plane of \mathcal{S}_t . The coefficients are of the form

$$\sigma^{\alpha\beta} = \chi(\rho, \rho_b) \Delta\mu_{\text{ATP}} g^{\alpha\beta}. \quad (91)$$

Using the covariant analogue of the gradient operator $\nabla = \mathbf{R}_{,\mu} g^{\mu\nu} \partial_\nu$, the corresponding force (per unit area) is given by

$$\begin{aligned} \nabla \cdot \sigma &= \sigma^{\alpha\beta}_{,\nu} g^{\mu\nu} (\mathbf{R}_{,\mu} \cdot \mathbf{R}_{,\alpha}) \mathbf{R}_{,\beta} + \sigma^{\alpha\beta} g^{\mu\nu} (\mathbf{R}_{,\mu} \cdot \mathbf{R}_{,\alpha\nu}) \mathbf{R}_{,\beta} + \sigma^{\alpha\beta} g^{\mu\nu} (\mathbf{R}_{,\mu} \cdot \mathbf{R}_{,\alpha}) \mathbf{R}_{,\beta\nu} \\ &= \sigma^{\alpha\beta}_{,\alpha} \mathbf{R}_{,\beta} + \sigma^{\alpha\beta} \Gamma_{\alpha\nu}^\nu \mathbf{R}_{,\beta} + \sigma^{\alpha\beta} \left(\Gamma_{\alpha\beta}^\gamma \mathbf{R}_{,\gamma} + b_{\alpha\beta} \hat{\mathbf{n}} \right) \\ &= \sigma^{\alpha\beta}_{;\alpha} \mathbf{R}_{,\beta} + \sigma^{\alpha\beta} b_{\alpha\beta} \hat{\mathbf{n}}, \end{aligned} \quad (92)$$

where the Gauss relation (27) and the definition of the covariant derivative have been used.

Since the active stress relies on the density of ‘‘bound’’ or ‘‘activated’’ myosin, an auxiliary equation for the time dependence of $\rho_b(u, t) = m_b(u, t)/\sqrt{g}(u, t)$ is needed (here, m_b is the local mass of Myosin at time $t = 0$). We write the continuity equation for a conserved scalar field on a deformable manifold, including Langmuir-like source and sink terms:

$$\partial_t \rho_b + (\rho_b v^\alpha)_{;\alpha} - \rho_b v^{(n)} 2H = k_{\text{on}} - k_{\text{off}} \rho_b. \quad (93)$$

At this stage we do not specify the functional dependence of k_{on} and k_{off} which may be related to mechanical properties such as strains, strain-rates, stresses or forces (gradients of stress). In the example calculation, both k_{on} and k_{off} are taken to be constant. [Note that, unlike (52), the convective term $v^\alpha (\rho_b)_{;\alpha}$ cannot be ignored, even if the initial mass distribution (at $t = 0$) was homogeneous, due to the presence of source and sink terms].

XV. QUASI-1D EXAMPLE

A. Setup

Consider the following ‘‘quasi-1D’’ example. At time $t = 0$, the tissue is in a flat steady state (*i.e.*, $b_{\alpha\beta}(u, 0) = 0$ for all u). Although flat, the tissue is active: there is a homogeneous steady state concentration of bound myosin $\rho_b(u, 0)$, which leads to homogeneous contractile stresses σ . If there is no opposing force applied at the tissue boundary, then the contractile stresses are balanced by the restoring forces associated with the mechanical response of the cells.

For convenience, we choose to apply a force at the boundary such that the (homogeneous) metric at steady state, $g_{\alpha\beta}(u, 0)$, is the same as the rest metric $g_{\alpha\beta}^\dagger$. We are then free to choose the coordinates u such that $g_{\alpha\beta}(u, 0) = g_{\alpha\beta}^\dagger = \delta_{\alpha\beta}$. [Note that, formally, we say $\mathcal{S}_{t=0}$ is isometric to \mathbb{R}^2 . This permits the decomposition $\mathbf{R}_t = \Gamma_t \circ \gamma$, where $\gamma : \mathbb{R}^2 \rightarrow \mathbb{R}^3$ maps points u to \mathcal{S}_0 , and $\Gamma_t : \mathbb{R}^3 \rightarrow \mathbb{R}^3$ is a diffeomorphism between positions of a give point u at different times. The coefficients $\epsilon_{\alpha\beta}$ are then just given by $\mathbf{R}_t^* \epsilon^{\mathbb{R}^3} (\vec{e}_\alpha, \vec{e}_\beta) = g_{\alpha\beta} - \delta_{\alpha\beta}$, where $\epsilon^{\mathbb{R}^3} = [(\psi_0^* - \psi_{-t}^*) \mathbf{I}]$ is the Green-Lagrange strain in \mathbb{R}^3 , and $\mathbf{I} = \delta_{ij} dx^i \otimes dx^j$ is the first fundamental form of three dimensional Euclidean space.].

Using a Monge-like parameterisation, we then consider the linear response of the tissue to small perturbations. We define the three functions R_t^i that comprise the embedding $\mathbf{R}_t : \mathbb{R}^2 \rightarrow \mathbb{R}^3$, as:

$$x^1 = R_t^1(u) = u^1 + \varepsilon \omega(u^1, t), \quad x^2 = R_t^2(u) = u^2, \quad \text{and} \quad x^3 = R_t^3(u) = \varepsilon h(u^1, t), \quad (94)$$

where $\varepsilon \ll 1$ is a small dimensionless number. For notational simplicity, let u^1 and u^2 be replaced by Euclidean x and y , respectively. We have

$$\mathbf{R}(x, y, t) = \begin{pmatrix} x + \varepsilon \omega(x, t) \\ y \\ \varepsilon h(x, t) \end{pmatrix}, \quad \mathbf{R}_{,1} = \begin{pmatrix} 1 + \varepsilon \partial_x \omega \\ 0 \\ \varepsilon \partial_x h \end{pmatrix}, \quad \text{and} \quad \mathbf{R}_{,2} = \begin{pmatrix} 0 \\ 1 \\ 0 \end{pmatrix}. \quad (95)$$

To linear order,

$$g_{\alpha\beta} \simeq \begin{pmatrix} 1 + 2\varepsilon \partial_x \omega & 0 \\ 0 & 1 \end{pmatrix}, \quad g^{\alpha\beta} \simeq \begin{pmatrix} 1 - 2\varepsilon \partial_x \omega & 0 \\ 0 & 1 \end{pmatrix}, \quad \text{and} \quad \hat{\mathbf{n}} \simeq \begin{pmatrix} -\varepsilon \partial_x h \\ 0 \\ 1 \end{pmatrix}. \quad (96)$$

Moreover, since

$$\mathbf{R}_{,11} = \begin{pmatrix} \varepsilon \partial_x^2 \omega \\ 0 \\ \varepsilon \partial_x^2 h \end{pmatrix}, \quad \text{and} \quad \mathbf{R}_{12} = \mathbf{R}_{21} = \mathbf{R}_{22} = 0, \quad (97)$$

then

$$b_{\alpha\beta} \simeq \begin{pmatrix} \varepsilon \partial_x^2 h & 0 \\ 0 & 0 \end{pmatrix} \implies H \simeq \frac{\varepsilon \partial_x^2 h}{2}, \text{ and } K \simeq 0. \quad (98)$$

B. Mechanical response

Working to lowest order in ε , the apical strains are given by

$$\epsilon_{\alpha\beta} \simeq \epsilon^{\alpha\beta} \simeq \begin{pmatrix} 2\varepsilon \partial_x \omega & 0 \\ 0 & 0 \end{pmatrix}, \quad \text{Tr}_g(\epsilon_{\alpha\beta}) = \text{Tr}_g(\epsilon^{\alpha\beta}) \simeq 2\varepsilon \partial_x \omega, \text{ and } \bar{\epsilon}_{\alpha\beta} \simeq \bar{\epsilon}^{\alpha\beta} \simeq \begin{pmatrix} \varepsilon \partial_x \omega & 0 \\ 0 & -\varepsilon \partial_x \omega \end{pmatrix}, \quad (99)$$

where $\bar{\epsilon}_{\alpha\beta} = \epsilon_{\alpha\beta} - g_{\alpha\beta} \text{Tr}_g(\epsilon_{\alpha\beta})/2$ is the traceless-symmetric part of $\epsilon_{\alpha\beta}$. The overall contribution of apical faces to the effective free energy is, to lowest order,

$$C^{\alpha\beta\gamma\delta} \epsilon_{\alpha\beta} \epsilon_{\gamma\delta} = \mu \bar{\epsilon}_{\alpha\beta} \bar{\epsilon}^{\alpha\beta} + \lambda [\text{Tr}_g(\epsilon_{\alpha\beta})]^2 = 4\varepsilon^2 \left(\lambda_A + \frac{\mu_A}{2} \right) (\partial_x \omega)^2 + O(\varepsilon^3). \quad (100)$$

Due to the volume constraint (70), we have

$$\ell = V(1 - 2\varepsilon \partial_x \omega) + O(\varepsilon^2), \quad (101)$$

which assumes $|\ell \partial_x^2 h|/2 = \varepsilon \ll 1$. Substituting into the expressions for the basal metric and inverse metric [Eqs. (65) and (66), respectively] and keeping only the terms to linear order in ε , the resultant strains are

$$\epsilon_{\alpha\beta}^B \simeq \epsilon^{\alpha\beta} \simeq \begin{pmatrix} \varepsilon 2 (\partial_x \omega + V \partial_x^2 h) & 0 \\ 0 & 0 \end{pmatrix}, \quad \text{Tr}_g(\epsilon_{\alpha\beta}^B) = \text{Tr}_g(\epsilon_{\alpha\beta}^B) \simeq \varepsilon 2 (\partial_x \omega + V \partial_x^2 h), \quad (102)$$

and

$$\bar{\epsilon}_{\alpha\beta}^B \simeq \bar{\epsilon}_{\alpha\beta}^B \simeq \begin{pmatrix} \varepsilon \left(\partial_x \omega + \frac{V \partial_x^2 h}{2} \right) & 0 \\ 0 & -\varepsilon \left(\partial_x \omega + \frac{V \partial_x^2 h}{2} \right) \end{pmatrix}. \quad (103)$$

The overall contribution of basal elasticity to the free energy is, to lowest order,

$$C_{\text{B}}^{\alpha\beta\gamma\delta} \epsilon_{\alpha\beta}^B \epsilon_{\gamma\delta}^B = \mu_{\text{B}} \bar{\epsilon}_{\alpha\beta}^B \bar{\epsilon}_{\alpha\beta}^B + \lambda_{\text{B}} [\text{Tr}_g(\epsilon_{\alpha\beta}^B)]^2 = \varepsilon^2 \left(\lambda_{\text{B}} + \frac{\mu_{\text{B}}}{2} \right) 4 (\partial_x \omega + V \partial_x^2 h)^2 + O(\varepsilon^3). \quad (104)$$

We may then compute π and ψ according to (75) and (76), giving

$$\pi^{11} = \frac{\kappa}{2} [(\ell^\dagger)^2 - V^2] + 4\varepsilon \left\{ \partial_x \omega \left(\lambda_{\text{A}} + \lambda_{\text{B}} + \frac{\mu_{\text{A}}}{2} + \frac{\mu_{\text{B}}}{2} + \frac{\kappa}{4} [2V^2 - (\ell^\dagger)^2] \right) + V \partial_x^2 h \left(\lambda_{\text{B}} + \frac{\mu_{\text{B}}}{2} \right) \right\} + O(\varepsilon^2), \quad (105)$$

and

$$\psi^{11} = 8\varepsilon V \left[(V \partial_x^2 h + 2 \partial_x \omega) \left(\lambda_{\text{B}} + \frac{\mu_{\text{B}}}{2} \right) \right] + O(\varepsilon^2), \quad (106)$$

respectively, where $\pi^{22} = \pi^{12} = \pi^{21} = \psi^{22} = \psi^{12} = \psi^{21} = 0$. Writing $\mathbf{f}_{\text{el}} = -\delta\mathcal{F}/\delta\mathbf{R}$ and invoking (86), we see that the components of the resulting passive forces are

$$f_{\text{el}}^1 = 4\varepsilon \left\{ \partial_x^2 \omega \left(\lambda_{\text{A}} + \lambda_{\text{B}} + \frac{\mu_{\text{A}}}{2} + \frac{\mu_{\text{B}}}{2} + \frac{\kappa}{4} [2V^2 - (\ell^\dagger)^2] \right) + V \partial_x^3 h \left(\lambda_{\text{B}} + \frac{\mu_{\text{B}}}{2} \right) \right\} + O(\varepsilon^2), \quad (107)$$

and

$$f_{\text{el}}^{(n)} = \varepsilon \left\{ \frac{\kappa}{2} [(\ell^\dagger)^2 - V^2] \partial_x^2 h - 8V \left[(V \partial_x^4 h + \partial_x^3 \omega) \left(\lambda_{\text{B}} + \frac{\mu_{\text{B}}}{2} \right) \right] \right\} + O(\varepsilon^2), \quad (108)$$

where $f_{\text{el}}^2 = 0$.

C. Active contractility

Writing $\rho(x, t) = \rho^{(0)} + \varepsilon \rho^{(1)}(x, t) + O(\varepsilon^2)$ and $\rho_b(x, t) = \rho_b^{(0)} + \varepsilon \rho_b^{(1)}(x, t) + O(\varepsilon^2)$, Eqn. (91) may be expanded as a power series in ε . Before doing so, we identify $\rho(x, 0)$ with $\rho^{(0)}$, *i.e.*, the steady state number density of cells per unit area is the same as that at time $t = 0$. From here, it is straightforward to show that $\rho^{(1)} = -\rho^{(0)} \partial_x \omega$ (see §XI C). Similarly, from the continuity equation for ρ_b [Eq. (93)] we see that $\rho_b^{(0)} = k_{\text{on}}/k_{\text{off}} =: k$. Expanding (91), we have

$$\sigma^{\alpha\beta} = \chi^{(0)} \Delta\mu_{\text{ATP}} \delta^{\alpha\beta} + \varepsilon \Delta\mu_{\text{ATP}} \left[\chi^{(0)} (g^{\alpha\beta})^{(1)} + \frac{\partial\chi}{\partial\rho_b} \Big|_{\varepsilon=0} \rho_b^{(1)} \delta^{\alpha\beta} - \frac{\partial\chi}{\partial\rho} \Big|_{\varepsilon=0} \rho^{(0)} \partial_x \omega \delta^{\alpha\beta} \right] + O(\varepsilon^2), \quad (109)$$

where $\chi^{(0)} = \chi^{(0)}(\rho^{(0)}, k)$. Writing $\mathbf{f}_{\text{ac}} = \nabla \cdot \sigma$ and invoking (92), the components of the resulting active forces are

$$f_{\text{ac}}^1 = \varepsilon \Delta\mu_{\text{ATP}} \left[\partial_x \rho_b^{(0)} \frac{\partial\chi}{\partial\rho_b} \Big|_{\varepsilon=0} - \partial_x^2 \omega \left(\chi^{(0)} + \rho^{(0)} \frac{\partial\chi}{\partial\rho} \Big|_{\varepsilon=0} \right) \right] + O(\varepsilon^2), \quad (110)$$

and

$$f_{\text{ac}}^{(n)} = \varepsilon \Delta\mu_{\text{ATP}} \chi^{(0)} \partial_x^2 h + O(\varepsilon^2), \quad (111)$$

where $f_{\text{ac}}^2 = 0$.

D. Embedding fluid

The epithelium is impermeable, and we therefore assume a “no-slip” condition between \mathcal{S}_t and the embedding fluid. The movement of \mathcal{S}_t , specified by the velocities $\mathbf{v}(u, t) = \partial \mathbf{R}(u, t)/\partial t$, is therefore related to the forces $\mathbf{f} = \mathbf{f}_{\text{el}} + \mathbf{f}_{\text{ac}}$ (§XV B and §XV C) via convolution with the Oseen tensor [21]:

$$\mathbf{v}(\mathbf{R}(u, t)) = \int_{\mathbb{R}^2} du' \mathbf{O}(\mathbf{R}(u', t) - \mathbf{R}(u, t)) \cdot \mathbf{f}(\mathbf{R}(u', t)), \quad (112)$$

where the components of \mathbf{O} in the local basis $\mathbf{e}_i = \{\mathbf{R}_{,1}, \mathbf{R}_{,2}, \hat{\mathbf{n}}\}$, are given by $\mathbf{O}^{ij} = \Lambda_p^i \Lambda_p^j \mathbf{O}_{\mathbb{E}^3}^{pq}$. Here, $\mathbf{O}_{\mathbb{E}^3}^{ij}$ are the usual components of the Oseen tensor

$$\mathbf{O}_{\mathbb{E}^3}^{ij}(\mathbf{x}) = \frac{1}{8\pi\eta|\mathbf{x}|} \left(\delta^{ij} + \frac{x^i x^j}{|\mathbf{x}|^2} \right), \quad (113)$$

where $\mathbf{x} = x^i \hat{\mathbf{e}}_i^{\mathbb{E}^3}$, such that $\hat{\mathbf{e}}_i^{\mathbb{E}^3} = \{\hat{\mathbf{x}}, \hat{\mathbf{y}}, \hat{\mathbf{z}}\}$ is the usual Euclidean basis. The matrix Λ is prescribed by the relation $\mathbf{e}_i = \Lambda_p^j \hat{\mathbf{e}}_j^{\mathbb{E}^3}$, and can be computed given an explicit embedding. Using (94) results in a power series expansion of \mathbf{O} in terms ε . However, since \mathbf{f} has no $O(\text{const.})$ term [ensuring that $\mathbf{v} = 0$ when $\varepsilon = 0$, *i.e.*, at steady state] then the $O(\varepsilon)$ contribution to \mathbf{v} is just

$$\mathbf{v}^{(1)}(\mathbf{R}(u, t)) = \int_{\mathbb{R}^2} du' \mathbf{O}^{(0)}(\mathbf{R}(u', t) - \mathbf{R}(u, t)) \cdot \mathbf{f}^{(1)}(\mathbf{R}(u', t)). \quad (114)$$

The lack of a zeroth order term also implies

$$g^{\alpha\beta} \mathbf{R}_{,\beta} \cdot \mathbf{v} = \mathbf{v} \cdot \hat{\mathbf{e}}_\alpha^{\mathbb{E}^3} + O(\varepsilon^2) \quad \text{and} \quad \hat{\mathbf{n}} \cdot \mathbf{v} = \mathbf{v} \cdot \hat{\mathbf{e}}_3^{\mathbb{E}^3} + O(\varepsilon^2). \quad (115)$$

That is, up to $O(\varepsilon^2)$, the Euclidean components of the velocity field are the same as those expressed in the basis local to \mathcal{S}_t . As a result, we may write the following component-wise expression:

$$\left[v^{(1)} \right]^i(x, y; t) = \int_{\mathbb{R}^2} du' \left[\mathbf{O}^{(0)} \right]_j^i(x' - x, y' - y) \left[f^{(1)} \right]^j(x', y'; t). \quad (116)$$

where there is an implicit sum over j , and the components of $\mathbf{O}^{(0)}$ are

$$\left[\mathbf{O}^{(0)} \right]_j^i(x, y) = \frac{1}{8\pi\eta(x^2 + y^2)^{1/2}} \left[\begin{pmatrix} 1 & 0 & 0 \\ 0 & 1 & 0 \\ 0 & 0 & 1 \end{pmatrix} + \frac{1}{(x^2 + y^2)} \begin{pmatrix} xx & xy & 0 \\ yx & yy & 0 \\ 0 & 0 & 0 \end{pmatrix} \right]. \quad (117)$$

Using the notation

$$\mathcal{F}_{\mathbf{q}}\{\varphi\} = \int_{-\infty}^{\infty} dx \int_{-\infty}^{\infty} dy \varphi e^{-i\mathbf{q}\cdot\mathbf{r}}, \quad (118)$$

where $\mathbf{r} = (x, y)^\top$ and $\mathbf{q} = (q_x, q_y)^\top$, we may take the two-dimensional Fourier transform of (116). The result is that

$$\left[\mathcal{F}_{\mathbf{q}} \left\{ v^{(1)} \right\} \right]^i = \left[\mathcal{F}_{\mathbf{q}} \left\{ \mathbf{O}^{(0)} \right\} \right]_j^i \left[\mathcal{F}_{\mathbf{q}} \left\{ f^{(1)} \right\} \right]^j. \quad (119)$$

To compute the Fourier transform of the (zeroth order) Oseen tensor, we may exploit the fact that $\mathbf{O}_{ij}^{(0)} = \mathbf{O}_{\alpha\beta}^{(0)} \oplus \mathbf{O}_{33}^{(0)}$ and hence $\mathcal{F}_{\mathbf{q}} \left\{ \mathbf{O}^{(0)} \right\} = \mathcal{F}_{\mathbf{q}} \left\{ \mathbf{O}_{\alpha\beta}^{(0)} \right\} \oplus \mathcal{F}_{\mathbf{q}} \left\{ \mathbf{O}_{33}^{(0)} \right\}$, where

$$\mathbf{O}_{\alpha\beta}^{(0)}(x, y) = \frac{1}{8\pi\eta|\mathbf{r}|} \left(\delta_{\alpha\beta} + \frac{r_\alpha r_\beta}{|\mathbf{r}|^2} \right), \quad (120)$$

and $\mathbf{O}_{33}^{(0)} = 1/8\pi\eta|\mathbf{r}|$. To compute the necessary Fourier transforms, we use the following three facts [30]:

1. The n -dimensional Fourier transform of a homogeneous function of degree λ is a homogeneous function of degree $-\lambda - n$.
2. The Fourier transform of a ‘‘radial’’ function (*i.e.*, depending on distance rather than absolute position) is also a radial function.
3. That $\mathcal{F}_{\mathbf{q}} \left\{ \text{Tr} \mathbf{O} \right\} = \text{Tr} \mathcal{F}_{\mathbf{q}} \left\{ \mathbf{O} \right\}$.

Consider first $\mathcal{F}_{\mathbf{q}} \left\{ \mathbf{O}_{\alpha\beta}^{(0)} \right\}$, which, via linearity, is just the sum of $\mathcal{F}_{\mathbf{q}} \left\{ \frac{\delta_{\alpha\beta}}{8\pi\eta|\mathbf{r}|} \right\}$ and $\mathcal{F}_{\mathbf{q}} \left\{ \frac{r_\alpha r_\beta}{8\pi\eta|\mathbf{r}|^3} \right\}$. Using 1. and 2. above, we have,

$$\mathcal{F}_{\mathbf{q}} \left\{ \frac{\delta_{\alpha\beta}}{8\pi\eta|\mathbf{r}|} \right\} = \frac{\delta_{\alpha\beta}}{8\pi\eta} \int_{\mathbb{R}^2} d\mathbf{r} e^{-i\mathbf{q}\cdot\mathbf{r}} \frac{1}{|\mathbf{r}|} = \frac{c_1 \delta_{\alpha\beta}}{8\pi\eta|\mathbf{q}|}, \quad (121)$$

and

$$\mathcal{F}_{\mathbf{q}} \left\{ \frac{r_\alpha r_\beta}{8\pi\eta|\mathbf{r}|^3} \right\} = -\frac{\partial_{q_x} \partial_{q_y}}{8\pi\eta} \int_{\mathbb{R}^2} d\mathbf{r} e^{-i\mathbf{q}\cdot\mathbf{r}} \frac{1}{|\mathbf{r}|^3} = -\frac{c_2 \partial_{q_x} \partial_{q_y} |\mathbf{q}|}{8\pi\eta} = \frac{c_2}{8\pi\eta} \left(\delta_{\alpha\beta} - \frac{q_\alpha q_\beta}{|\mathbf{q}|^2} \right). \quad (122)$$

The constants c_1 and c_2 can be fixed by invoking 3., above, which implies that $c_1 = c_2 = 2\pi$, and hence

$$\mathcal{F}_{\mathbf{q}} \left\{ \mathbf{O}_{\alpha\beta}^{(0)} \right\} = \frac{1}{4\eta|\mathbf{q}|} \left(2\delta_{\alpha\beta} - \frac{q_\alpha q_\beta}{|\mathbf{q}|^2} \right). \quad (123)$$

Similarly, it is straightforward to show that $\mathcal{F}_{\mathbf{q}} \left\{ \mathbf{O}_{33}^{(0)} \right\} = 1/4\eta|\mathbf{q}|$, and therefore

$$\mathcal{F}_{\mathbf{q}} \left\{ \mathbf{O}_{ij}^{(0)} \right\} = \frac{1}{4\eta|\mathbf{q}|} \left[\begin{pmatrix} 2 & 0 & 0 \\ 0 & 2 & 0 \\ 0 & 0 & 1 \end{pmatrix} + \frac{1}{|\mathbf{q}|^2} \begin{pmatrix} q_x q_x & q_x q_y & 0 \\ q_y q_x & q_y q_y & 0 \\ 0 & 0 & 0 \end{pmatrix} \right]. \quad (124)$$

Turning our attention to $\mathcal{F}_{\mathbf{q}} \left\{ \mathbf{f}^{(1)} \right\}$, we note that $\mathbf{f}^{(1)}$ is not a function of y , and therefore $\mathcal{F}_{\mathbf{q}} \left\{ \mathbf{f}^{(1)} \right\} = \mathcal{F}_{q_x} \left\{ \mathbf{f}^{(1)} \right\} \delta(-q_y/2\pi)$. Dropping the subscript x for convenience, and using the fact that $[\mathbf{f}^{(1)}]^2 = 0$, it can be shown that

$$\mathcal{F}_q \left\{ \left[\mathbf{v}^{(1)} \right]^i \right\} = \frac{1}{4\eta q} \mathcal{F}_q \left\{ \left[\mathbf{f}^{(1)} \right]^i \right\}. \quad (125)$$

E. Linear stability

For the general case of arbitrary deformations, there are five dynamical variables: two each for $g_{\alpha\beta}$ and $b_{\alpha\beta}$ (due to the Gauss-Codazzi relations) plus the scalar density ρ_b . However, when restricted to quasi-1D deformations, the number of degrees-of-freedom is reduced to three. In our case, natural choices are the local surface area measure \sqrt{g} , the mean curvature H , and ρ_b . The corresponding dynamical equations are given by (49), (62) and (93). Here, since $\mathbf{v} = \varepsilon \mathbf{v}^{(1)}(x, t) + O(\varepsilon^2)$ and $\hat{e}_2^{\mathbb{E}^3} \cdot \mathbf{v}^{(1)} = [\mathbf{v}^{(1)}]^2 = 0$, at $O(\varepsilon)$ we have

$$\partial_t (\sqrt{g})^{(1)} = \partial_x [\mathbf{v}^{(1)}]^1 \implies -iq \partial_t \mathcal{F}_q \{\omega\} = -\frac{i}{4\eta} \mathcal{F}_q \left\{ [\mathbf{f}^{(1)}]^1 \right\}, \quad (126)$$

$$\partial_t H^{(1)} = \frac{1}{2} \partial_x^2 [\mathbf{v}^{(1)}]^3 \implies -\frac{q^2}{2} \partial_t \mathcal{F}_q \{h\} = -\frac{q}{8\eta} \mathcal{F}_q \left\{ [\mathbf{f}^{(1)}]^3 \right\}, \quad (127)$$

and

$$\partial_t \rho_b^{(1)} = -k \partial_x [\mathbf{v}^{(1)}]^1 - k_{\text{off}} \rho_b^{(1)} \implies \partial_t \mathcal{F}_q \{\rho_b^{(1)}\} = \frac{ik}{4\eta} \mathcal{F}_q \left\{ [\mathbf{f}^{(1)}]^1 \right\} - k_{\text{off}} \mathcal{F}_q \{\rho_b^{(1)}\}, \quad (128)$$

where, introducing the shorthand $A := \mu_A + \lambda_A$, $B := \mu_B + \lambda_B$, $\alpha := \partial\chi/\partial\rho_b|_{\varepsilon=0}$ and $\beta := \chi^{(0)} + \rho^{(0)} \partial\chi/\partial\rho|_{\varepsilon=0}$,

$$\mathcal{F}_q \left\{ [\mathbf{f}^{(1)}]^1 \right\} = \left(\beta \Delta\mu_{\text{ATP}} - 4 \left\{ A + B + \frac{\kappa}{4} \left[2V^2 - (\ell^\dagger)^2 \right] \right\} \right) q^2 \mathcal{F}_q \{\omega\} + i4q^3 V B \mathcal{F}_q \{h\} - iq \Delta\mu_{\text{ATP}} \alpha \mathcal{F}_q \left\{ \rho_b^{(1)} \right\}, \quad (129)$$

and

$$\mathcal{F}_q \left\{ [\mathbf{f}^{(1)}]^3 \right\} = -\left\{ \frac{\kappa}{2} \left[(\ell^\dagger)^2 - V^2 \right] + 8BV^2 q^2 + \Delta\mu_{\text{ATP}} \chi^{(0)} \right\} q^2 \mathcal{F}_q \{h\} - 8iq^3 V B \mathcal{F}_q \{\omega\}. \quad (130)$$

Eqs. (126), (127) and (128) can be written in terms of the following dimensionless variables: $\Lambda := A^2/\eta^2 \Delta\mu_{\text{ATP}}$, $\Phi := kA/\eta^2$, $\bar{\beta} := \beta \Delta\mu_{\text{ATP}}/A$, $\bar{\chi} := \chi^{(0)} \Delta\mu_{\text{ATP}}/A$, $\bar{q} := \ell^\dagger q$, $\bar{t} := \eta \Delta\mu_{\text{ATP}} t/A \ell^\dagger$, $\gamma := B/A$, $\bar{\kappa} := \kappa (\ell^\dagger)^2/A$, $\delta := V/\ell^\dagger$, $\overline{\mathcal{F}_q \{w\}} := \mathcal{F}_q \{w\} / (\ell^\dagger)^2$, $\overline{\mathcal{F}_q \{h\}} := \mathcal{F}_q \{h\} / (\ell^\dagger)^2$, and $\overline{\mathcal{F}_q \{\rho_b\}} := \mathcal{F}_q \{\rho_b\} / \beta \ell^\dagger$. Writing $\mathbf{x} = \left(\overline{\mathcal{F}_q \{w\}}, \overline{\mathcal{F}_q \{h\}}, \overline{\mathcal{F}_q \{\rho_b\}} \right)^\top$, the resulting matrix equation is given by $\partial_{\bar{t}} \mathbf{x} = \mathbf{M} \cdot \mathbf{x}$, where

$$\mathbf{M} = \begin{pmatrix} \Lambda \bar{q} \{\bar{\beta} - 4 [1 + \gamma + \bar{\kappa} (2\delta^2 - 1) / 4]\} / 4 & +i \Lambda \delta \gamma \bar{q}^2 & -i \Lambda \alpha \bar{\chi} / 4 \\ -2i \Lambda \delta \gamma \bar{q}^2 & -\Lambda \bar{q} [\bar{\beta} + 8\gamma \delta^2 \bar{q}^2 + \bar{\kappa} (1 - \delta^2) / 2] / 4 & 0 \\ i \Phi \bar{q}^2 \{\bar{\beta} - 4 [1 + \gamma + \bar{\kappa} (2\delta^2 - 1) / 4]\} / \bar{\beta} & -\Phi \delta \gamma \bar{q}^3 / \bar{\beta} & \Phi \alpha \bar{q} - \bar{k}_{\text{off}} \end{pmatrix}. \quad (131)$$

Focussing only on the variables δ , $\bar{\beta}$, and $\bar{\kappa}$, whose relative values can lead to sign changes of the coefficients of \mathbf{M} , we set all other variables equal to one (*i.e.*, $\Lambda = \Phi = \gamma = \bar{\chi} = \alpha = \bar{k}_{\text{off}} = 1$). We may then solve the corresponding eigenvalue equation $\mathbf{M} \cdot \hat{\mathbf{E}}^{(i)} = \hat{\mathbf{E}}^{(i)} \lambda_i$. Writing $\mathbf{x}(q, \bar{t}) = \sum_i \xi_i(q, \bar{t}) \hat{\mathbf{E}}^{(i)}(q)$, and substituting into the aforementioned matrix equation, implies $\xi_i(q, \bar{t}) = e^{\lambda_i(q) \bar{t}}$, hence solving for \mathbf{x} . To linear order in \bar{q} , the eigenvalues λ_i ($i = 1, 2, 3$) are real and given by:

$$\lambda_\alpha = -\frac{\bar{q}}{16} [16 + (3\delta^2 - 1) \bar{\kappa} + (-1)^\alpha [16 - 4\bar{\beta} - 3\bar{\kappa} + 5\delta^2 \bar{\kappa}]], \quad (132)$$

for $\alpha = 1, 2$, and $\lambda_3 = \bar{q} - 1$. The sign of (132), and hence the stability of the corresponding perturbation, changes according to two criteria

$$\delta^2 \bar{\kappa} - 2\bar{\beta} + \bar{\kappa} = 0, \quad \text{and} \quad 2\delta^2 \bar{\kappa} + 8 - \bar{\beta} - \bar{\kappa} = 0, \quad (133)$$

which correspond to the red-solid and blue-dashed lines of Fig. 4a of the main manuscript. We consider three cases, each of which is characterised by a different instability.

In all cases, a single eigenvalue, λ_1 , has the largest real part, irrespective of wave-number \bar{q} . For a \bar{q} corresponding to positive $\text{Re}[\lambda_1]$, the resulting instability is characterised by the coefficients of the eigenvector $\hat{\mathbf{E}}^1$, both real and imaginary parts. The relative growth rates of cosinusoidal perturbations $h(x, t)$, $\omega(x, t)$ and $\rho_b^{(1)}(x, t)$ are given by the

coefficients $\text{Re}[E_2^1]$, $\text{Re}[E_1^1]$, and $\text{Re}[E_3^1]$, respectively. Similarly, the relative growth rates of sinusoidal perturbations $h(x, t)$, $\omega(x, t)$ and $\rho_b^{(1)}(x, t)$ are given by the coefficients $\text{Im}[E_2^1]$, $\text{Im}[E_1^1]$, and $\text{Im}[E_3^1]$, respectively.

By analysing the fastest growing eigenvector in each of the cases of interest, the Monge parameterisation (94) may be used to visualise the corresponding deformations of cell junctions. Moreover, by invoking the cell-volume constraint (linearised, for consistency) to obtain cell thickness, we may construct a faithful representation of the tissue just after the onset of the instability (see Figs. 5, 6, and 7).

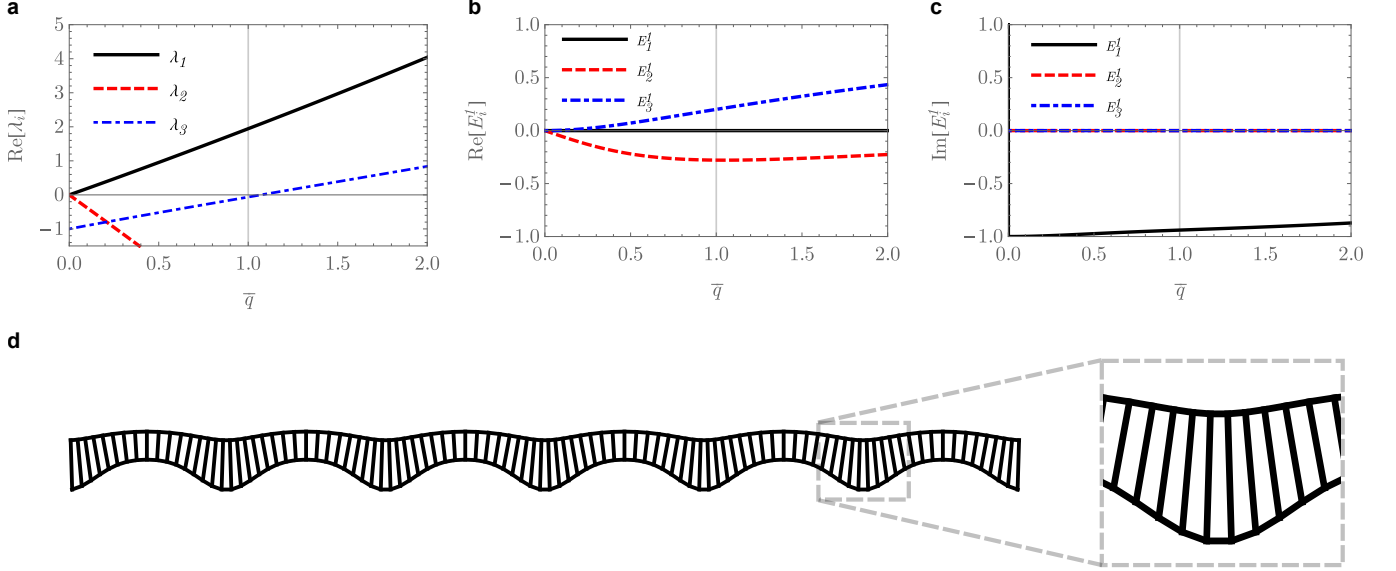


FIG. 5. (Color online). Invagination: $\delta = \sqrt{2}$, $\bar{\beta} = 15$, $\bar{\kappa} = 1/2$. At linear order, the $\text{Re}[\lambda_1]$ instability is unbounded [panel a]. However, we expect non-linearities to provide an effective cutoff, and therefore focus on characteristic behaviour at $\bar{q} = 1$. Cosinusoidal variations in $\rho_b(x, t)$ [panel b] [blue dot-dashed line] drive areas of apical contraction and expansion. Since $\delta > 1$, the steady-state corresponds to lateral faces that are already stretched. As a result, contraction of the apical faces corresponds to expansion of the basal faces (in addition to some further stretching of the lateral faces), due to the conservation of cell volume. At the cellular scale this gives rise to regular-prism to truncated-pyramid transitions [panel d] inset]. At a tissue level, this is seen as an invaginating phase [panel d] whose apical shape is a combination of both sinusoidal variations in $\omega(x, t)$ [panel c) black solid line] and cosinusoidal variations in $h(x, t)$ [panel b) red dashed line] (each phase-shifted by a factor of π).

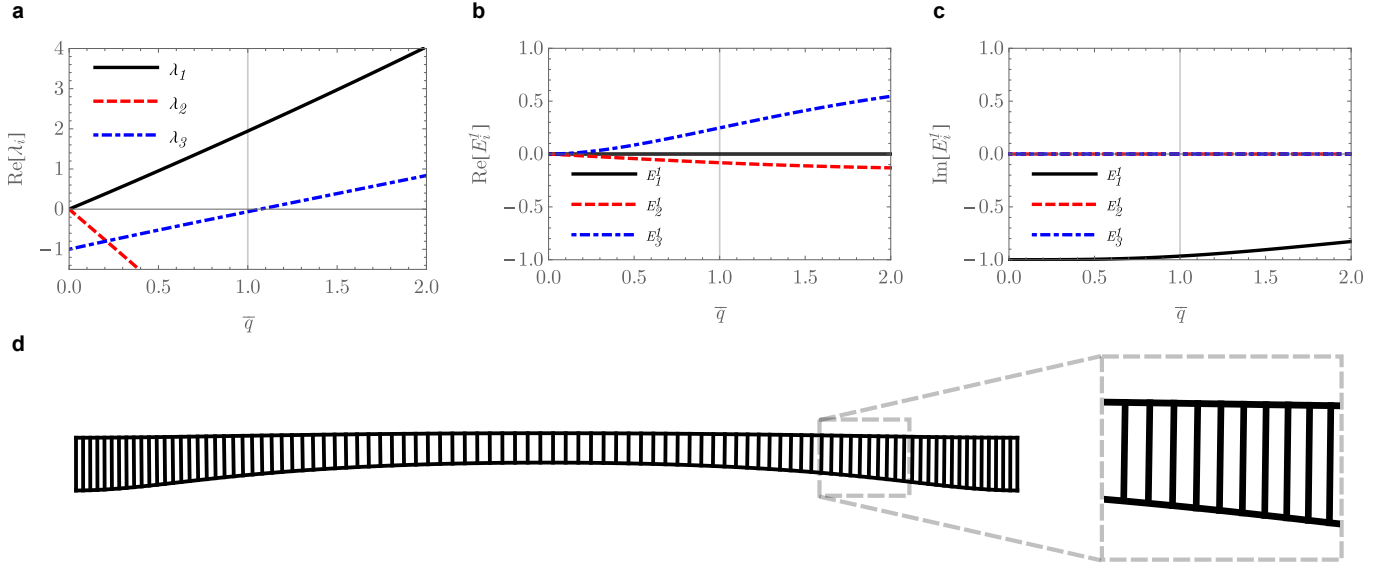


FIG. 6. (Color online). Sqaumous-to-columnar: $\delta = 1/4$, $\bar{\beta} = 15$, $\bar{\kappa} = 1/2$. At linear order, the $\text{Re}[\lambda_1]$ instability is unbounded [panel a]. However, we expect non-linearities to provide an effective cutoff, and therefore focus on characteristic behaviour at $\bar{q} = 1$ (although, for comparison with Fig. 5 the system has been scaled so that cells occupy the same volume, even though δ is different in the two cases). Cosinusoidal variations in $\rho_b(x, t)$ [panel b] blue dot-dashed line] drive areas of apical contraction and expansion. Since $\delta < 1$, the steady-state corresponds to lateral faces that are compressed. As a result, contraction of the apical faces corresponds to elongation of the lateral faces (in addition to an almost imperceptible expansion of basal faces), due to the conservation of cell volume. At the cellular scale, this gives rise to squamous to columnar transitions [panel d] inset]. At a tissue level, the apical shape is essentially flat [panel b] red dashed line], but with a thickness inversely proportional to π -phase-shifted sinusoidal variations in $\omega(x, t)$ [panel c] black solid line].

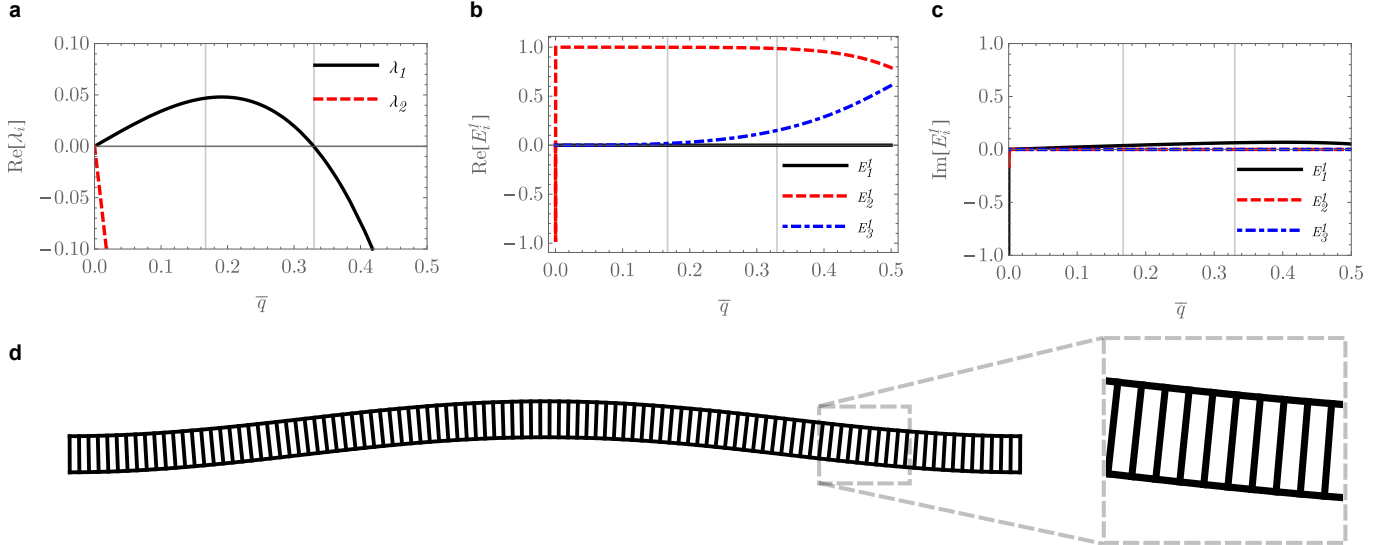


FIG. 7. (Color online). Constrained-buckling: $\delta = \sqrt{2}$, $\bar{\beta} = 15$, $\bar{\kappa} = 1/2$. The $\text{Re}[\lambda_1]$ instability bounded [panel a], with $\text{Re}[\lambda_1] \rightarrow 0$ as $\bar{q} \rightarrow 0$. For convenience, we focus on characteristic behaviour at $\bar{q} = 1/6$. Cosinusoidal variations in $\rho_b(x, t)$ [panel b] blue dot-dashed line] are negligible, and hence this is a passive instability, rather than an actively-driven one. Since $\delta > 1$, the steady-state corresponds to lateral faces that are already stretched. As a result, cosinusoidal variations in $h(x, t)$ [panel b] red dashed line] combined with negligible (sinusoidal) variations in $\omega(x, t)$ [panel c] black solid line] act to reduce lateral lengths at the expense of apical expansion, due to the conservation of cell volume.